Draft version August 21, 2022
Typeset using LaTeX **twocolumn** style in AASTeX631

Restart writing on July 11, 2022
Used high Galactic latitudes !
Comments welcome!

Hunting the possible Changing-Look Blazar Candidates in LSP-BL Lacs using Machine Learning

Shi-Ju Kang,[1] Yong-Gang Zheng,[2] Qingwen Wu,[3] and Junhui Fan[4]

[1]School of Physics and Electrical Engineering, Liupanshui Normal University, Liupanshui, Guizhou, 553004, People's Republic of China
[2]Department of Physics, Yunnan Normal University, Kunming, Yunnan, 650092, People's Republic of China
[3]Department of Astronomy, School of Physics, Huazhong University of Science and Technology, Wuhan, Hubei, 430074, People's Republic of China
[4]Center for Astrophysics, Guangzhou University, Guangzhou 510006, People's Republic of China

(Received May 28, 2022; Revised May 28, 2022; Accepted August 21, 2022)

Submitted to **ApJS**

ABSTRACT

Using a random forest (RF) supervised machine learning algorithm, these intrinsically FSRQs (flat spectrum radio quasars) that may be misclassified as BL Lacs (BL Lacerate objects) are hunted. In order to address the issue, based on the 4LAC-DR2 catalog, a sample of 1680 (1352+328) Fermi blazars with 23 parameters systematically selected on the direct observation is compiled. By studying the results for all of the different combinations of parameters, we found that there are 1, 5, 14, 35, 52, 39, 28, 2, or 2 parameter combinations with 5, 6, 7, 8, 9, 10, 11, 12, or 13 parameters in the RF generated models achieve the highest accuracy (Accuracy $\sim$ 98.89%). Using the combined classification results from the nine combinations of these optimal combinations of parameters, 113 actually BL Lac type sources (ABLLs) and possible 157 Changing-Look Blazar Candidates (CLBCs) that possible intrinsically FSRQs misclassified as BL Lacs are predicted; where, 58 remain without a clear prediction, for 328 LSP (low-synchrotron-peaked) BL Lacs reported in the high Galactic latitudes ($|b| > 10°$) 4LAC-DR2 catalog. Compared the ABLLs with CLBCs, we found that the CLBCs show a clear separation for ABLLs in the $logF_X$-Γ_{ph} plane. The CLBCs are located in the higher zone. Checked the Changing-Look (transition) Blazars (TCLBs) reported in the literatures, there are 34 of 35 LSP TCLBs are located in the transition zone. Therefore, we propose a B-to-F transition zone named "$B \to F$" zone, where the transition from BL Lacs to FSRQs will occur for some LSP BL Lacs.

Keywords: Blazars (164) — BL Lacertae objects (158) — Flat-spectrum radio quasars (2163)

Contents

1. Introduction 2
2. Random forests SML algorithms 4
3. Sample and Parameters Preparation 4
4. Optimal combinations of parameters and Results 7
5. Results comparison 13
6. Discussion and Conclusion 18
7. acknowledgment 20
A. An Online Changing-Look (Transition) Blazars Catalog 20
A.1. The TCLBs in Foschini et al. (2021) 20
A.2. The TCLBs in Peña-Herazo et al. (2021a) 21

Corresponding author: Shi-Ju Kang
kangshiju@alumni.hust.edu.cn

ynzyg@ynu.edu.cn

qwwu@hust.edu.cn

fjh@gzhu.edu.cn

A.3. The TCLBs in Ruan et al. (2014) 22
A.4. The TCLBs in Shaw et al. (2012) 23
A.5. The TCLBs in Ghisellini et al. (2011) 24
A.6. The TCLBs in other literatures 24

Some Note:

- **FSRQ: Flat-Spectrum Radio Quasar (EW-based classification, reported in 4LAC);**
- **BL Lac: BL Lac Object (EW-based classification, reported in 4LAC);**
- **CLB: Changing-Look Blazar;**
- **CLBC: CLB Candidate predicted in the work;**
- **ABLL: actually BL Lac type predicted in the work;**
- **TCLB: CLB (transition) blazars reported in the literatures.**

1. INTRODUCTION

Blazars are a peculiar sub-class of radio-loud active galactic nucleis (AGNs) with a relativistic jet pointed towards us, whose multi-wavelength spectral energy distributions (SEDs) dominantly originates from the non-thermal emission in the relativistic jet (Urry & Padovani 1995). The broadband SEDs normally exhibits a two-hump structure in the $\log\nu - \log\nu \mathrm{F}_\nu$ space. The lower energy bump usually originates from synchrotron radiation generated by non-thermal electrons in the jet, while the second bump mainly originates from inverse Compton (IC) scattering. Based on the peak frequency ($\nu_{\mathrm{p}}^{\mathrm{S}}$) of the lower energy bump, blazars are normally subclassified as low (LSP, e.g., $\nu_{\mathrm{p}}^{\mathrm{S}} < 10^{14}$ Hz), intermediate (ISP, e.g., 10^{14} Hz $< \nu_{\mathrm{p}}^{\mathrm{S}} < 10^{15}$ Hz) and high-synchrotron-peaked (HSP, e.g., $\nu_{\mathrm{p}}^{\mathrm{S}} > 10^{15}$ Hz) blazars (Abdo et al. 2010a; Fan et al. 2016). Most HSP and ISP blazars have been classified as BL Lac objects based on their optical spectra, while the LSP class contains both FSRQs and low-frequency-peaked BL Lac objects (Böttcher 2019; Prandini & Ghisellini 2022).

According to the strength of the optical spectral lines (e.g., equivalent width, EW, of the spectral line is greater or less than 5Å), blazars common come in two flavors: flat spectrum radio quasars (FSRQs) with the stronger emission lines (EW $\geq$ 5Å), and BL Lacerate objects (BL Lacs) that the spectral lines are fainter or even absent (EW $<$ 5Å) in their optical spectra (Stickel et al. 1991; Stocke et al. 1991). In addition, based on the sources with intrinsically weak or strong narrow emission lines (e.g., [O II] and [O III] EW), an analogous classification criterion also suggested by Landt et al. (2004) to discriminate them. What causes the intrinsic difference (different physical origins) between FSRQs and BL Lacs that has been been extensively explored. For instance, the dichotomy between FSRQ and BL Lac may be attributed to different accretion models (e.g., Cao 2002; Wang et al. 2002; Cao 2003; Dai et al. 2007; Ghisellini et al. 2009; Xu et al. 2009; Sbarrato et al. 2014; Chen et al. 2015; Chen 2018; Gardner & Done 2018; Boula et al. 2019; Mondal & Mukhopadhyay 2019; Keenan et al. 2021; Prandini & Ghisellini 2022 for more details and reference therein), which may provide different additional seed photons from outside of the jet (e.g., Ghisellini et al. 1998; Ghisellini 2016; Ghisellini et al. 2017; Prandini & Ghisellini 2022), where FSRQs with a standard cold accretion disk and BL Lacs have an advection-dominated accretion flow (ADAF; e.g., Yuan & Narayan 2014). Also, which may be attributed to the spin of a central black hole (e.g., see Bhattacharya et al. 2016; Gardner & Done 2018); and/or mass accretion rate on to the central black hole (e.g., see Boula et al. 2019); and/or both the mass accretion rate and magnetic field strength (e.g., see Mondal & Mukhopadhyay 2019).

The EW-based classification is simple to apply, and provide some clues or label/trace these sources with whether intrinsically strong (FSRQ) or weak (BL Lac) emission lines. However, EW-based classification remains an open question, challenged by observations. The possible bimodal distribution in the EW of the broad lines has not been detected. The EW-based classification with the EW value of 5 $\AA$ is rather arbitrary, for instance, in rest frame by Stickel et al. (1991) or observed-frame by Stocke et al. (1991). Blazar jet emission is extremely variable, definitely more than the thermal continuum and the emission lines. Hence, the line EW can dramatically vary from one state to another for the same source. So, the EW-based classification may have selection effects (e.g., Giommi et al. 2012, 2013; Padovani & Giommi 2015), and may lead to several misclassifications, since the the broad lines can be swamped (**diluted or hidden**) by a particularly strong (and possibly beamed) continuum (e.g., Ruan et al. 2014; Pasham & Wevers 2019). For instance, a blazar with intrinsically very luminous emission lines can temporarily appear as a BL Lac, with very small EW, if its jet flux happens to be more luminous than usual (e.g., Mishra et al. 2021). On the contrary, these transitional objects may show broad lines in the optical band when the continuum is low (e.g.,Ruan et al.

2014), where, during a particularly low state, a BL Lac can show emission lines with EW larger than the 5 Å limit (as it happened to BL Lac itself; Vermeulen et al. 1995; Corbett et al. 1996; Capetti et al. 2010). In addition, the EW-based classification is also affected by the strong non-thermal emission (e.g., Ghisellini et al. 2011), or a high Doppler boosting / jet bulk Lorentz factor variability (e.g., Bianchin et al. 2009a) , and the effect of high redshift (e.g., D'Elia et al. 2015; Stern & Poutanen 2014). Motivated by the observational background, some more physical classification are introduced: for instance, based on the different accretion rates of the two subclasses of blazars (e.g., Ghisellini et al. 2011; Sbarrato et al. 2012); based on the ionizing luminosity emitted from the accretion disc (e.g., Giommi et al. 2012, 2013). An intrinsically FSRQ is then misclassified as a BL Lac, and vice versa, which common labeled as transition blazars (e.g., Ghisellini et al. 2011; Shaw et al. 2012; Ruan et al. 2014), and also called "Changing-Look Blazar" (**CLB**, e.g., Bianchin et al. 2009a; Álvarez Crespo et al. 2016; Pasham & Wevers 2019; Mishra 2021; Foschini et al. 2021; Peña-Herazo et al. 2021a; Mishra et al. 2021; Peña-Herazo et al. 2021b; Pei et al. 2022; Zhang et al. 2022).

The LSP BL Lacs are a peculiar sub-class blazars. The differences between LSP BL Lacs and FSRQs or remaining BL Lacs (HSP and ISP) have been widely argued/ debated by some works (e.g., Linford et al. 2012). Some sources classified as LSP BL Lacs have strong emission lines, and are more strongly beamed than the rest of the BL Lac object population (e.g., Linford et al. 2012). Alternatively, sources classified as FSRQs may have weaker emission lines. The dichotomy between LSP BL Lac objects and FSRQ is complicated in the classification of blazars, which may be misclassified. Some of the LSP BL Lacs may not actually be BL Lacs (e.g.,Ghisellini et al. 2009; Giommi et al. 2012). In fact, it is possible that BL Lacertae itself is not actually a BL Lac object (Vermeulen et al. 1995), when its jet continuum is in a particularly low state, that can show emission lines with EW larger than the 5 Å. Some objects classified as LSP BL Lacs are actually FSRQs with exceptionally strong jet emission overpowering the emission lines (e.g., Ghisellini et al. 2012). The lack of obvious broad lines leads the astronomical community to misclassify some sources as BL Lac objects. In addition, some authors found that some parameters show a very broad distribution for LSP BL Lacs, which is somewhat bimodal (e.g., Fan & Wu 2019; Cheng et al. 2022). For example, the jet power of LSP BL Lacs shows a very broad bimodal distribution, which suggests that they may contain two populations, one is actually FSRQs with at high redshifts, others with a lower power located at low redshifts, similar to actually BL Lacs (e.g., Fan & Wu 2019). The distribution of the peak frequency of the synchrotron radiation, gamma-ray photon spectral index, and the X-band (8.4 GHz) flux density showed a similar bimodal for the LSP subclass; one distribution group similar to the BL Lacs and another similar to the FSRQs (Cheng et al. 2022). Which may indicate that some LSP-BL Lacs may belong to actually BL Lacs and others are essentially FSRQs, and vice versa.

Since the Fermi Gamma-ray Space Telescope was launched June 11, 2008, the Fermi Large Area Telescope (Fermi-LAT) First, Second, Third and Fourth Source Catalog of gamma-ray sources have regularly released, which common denoted as 1FGL (Abdo et al. 2010b), 2FGL (Nolan et al. 2012), 3FGL (Acero et al. 2015) or 4FGL (Abdollahi et al. 2020). Also, the new versions of the Fermi-LAT fourth source catalog have also been provided, recently, the Data Release 2 (4FGL-DR2, Ballet et al. 2020) and Data Release 3 (4FGL-DR3, Abdollahi et al. 2022). The corresponding First, Second, Third and Fourth Catalog of AGN Detected by the Fermi-LAT have also regularly released (1LAC, Abdo et al. 2010c; 2LAC, Ackermann et al. 2011; 3LAC, Ackermann et al. 2015; and 4LAC, Ajello et al. 2020). Recently, a new version of the Fourth Catalog of AGN by the Fermi-LAT – Data Release 2 (4LAC-DR2, Lott et al. 2020) is reported, which is by far the largest gamma-ray AGN source group. The 4LAC-DR2 includes 3131 sources, with 3063 blazars (707 FSRQs, 1236 BL Lacs, 1120 BCUs), and 68 other AGNs, located at high Galactic latitudes ($|b| > 10°$). Of which 3063 blazars include 1388 LSP, 474 ISP, 506 HSP, and 695 no SED class; 380 sources, with 374 blazars (37 FSRQs, 72 BL Lacs, 265 BCUs), and 6 other AGNs, located at low Galactic latitudes ($|b| < 10°$). Of which 374 blazars include 117 LSP, 18 ISP, 37 HSP, and 202 no SED class. The large sample and abundant observational information provide us with a unique and excellent opportunity to study the physics of the γ-ray emissions of blazars (e.g., Paliya et al. 2021; Pei et al. 2022, and so on).

In addition, with a testimony to the substantial follow-up observational efforts, the optical classifications of some blazars is also continuously confirmed and updated (reclassification) in a new version of Fermi catalog. Some probably transitional objects are reported in the different versions of the Fermi source catalog. For instance, relative to 3LAC (Ackermann et al. 2015), the 4LAC (Ajello et al. 2020) reported that optical classifications of eight sources have changed from a FSRQ to a BL Lac (RGB J0250+172, NVSS J040324242946, GB6 J0941+2721, 2MASS J11303636+1018245, PKS 1144 379, 4C +15.54, TXS 1951115, PKS 2233173) and three sources from a B L Lac to a FSRQ (PMN J07090255, B2 2234 +28A, TXS 2241+406); also, 3FGL J0202.3+0851 was classified as an FSRQ in 3LAC from a BL Lac in 1LAC (Ackermann et al. 2015; Acero et al. 2015), etc. .

In the 4LAC catalog (Ajello et al. 2020), they reported that there is an expected region for objects that might be transitioning between being FSRQs and BL Lacs, based on the $\nu_{\rm p}^{\rm S}$ and their photon index distributions of LSP BL Lacs and FSRQs that are overlap. For the six such transitioning objects found in Ruan et al. (2014), Five of them, all of the LSP subclass, are present in 4LAC. So, some LSP BL Lacs are more likely to be transitioning (changing-look type) objects which intrinsically are FSRQs than other sources. Motivated by these observational background, we employ a Random Forest (RF) supervised machine learning (SML) algorithms, and try to diagnose/evaluate those sources that were intrinsically FSRQs that were misclassified as LSP BL Lac using the 4FGL catalog, to hunt the possible transition region for the objects that might be transitioning between being FSRQs and BL Lacs, based on the direct observational gamma-ray properties. Section 2 introduces the Random Forest supervised machine learning algorithms. The method used to select the parameters and data sample from the catalog is described in Section 3. The Optimal combinations of parameters and classification results are reported in Section 4. A comparison with other results is presented in Section 5. The discussion and conclusion are shown in Section 6.

2. RANDOM FORESTS SML ALGORITHMS

Random forests algorithms is a popular, well established SML algorithms, which has been widely used in astronomical research (e.g., see Baron 2019; Feigelson & Babu 2012; Kabacoff 2015 for the reviews). In the work, the RF algorithm was employed due to its high prediction accuracy in previous work (e.g., see Kang et al. 2019a,b). The original RF proposal (Breiman 2001), which has evolved over time, transforms a training sample into a large collection of decisions trees (e.g., a forest). These trees are used to conduct an extensive voting scheme, which enhances the classification and the prediction accuracy of the model. The RF algorithm has numerous advantages, including accuracy, scalability, and the ability to address challenging datasets. In terms of accuracy, the RF approach has outperformed alternative approaches, for example, decision trees (Fernández-Delgado et al. 2014). This approach has been applied to a very large astronomical dataset (Breiman et al. 2003). RF successfully builds predictive models for uneven datasets, for example, those with large amounts of missing data or a relatively limited ratio of observations in comparison to the number of variables. The RF approach also generates out-of-bag error rates, in addition to measures indicating the relative importance of the variables. However, due to the large number of trees (default 500 trees), it is difficult to understand the classification rules and make communications.

Many software packages are available for RF algorithms. The randomForest package in R[1] (Liaw & Wiener 2002) (R version 4.1.2, R Core Team 2022) is selected and used to fit a random forest in the work. Additionally, the accuracy of the model is calculated using the $classAgreement()$ function in the e1071 package (Meyer et al. 2021). An R package “snowfall” is employed to make parallel programming (Knaus 2015).

3. SAMPLE AND PARAMETERS PREPARATION

The 4LAC-DR2 (arXiv:2010.08406[2,3] was released on October 16, 2020) includes 3131 sources, with 3063 blazars (707 FSRQs, 1236 BL Lacs, 1120 BCUs), and 68 other AGNs, located at high Galactic latitudes ($|b| > 10°$), Of which 3063 blazars include 1388 LSP, 474 ISP, 506 HSP, and 695 no SED class. From the high Galactic latitudes 4LAC-DR2 FITS tables:“table-4LAC-DR2-h.fits”[4], we select 1680 blazars that have known optical classifications (FSRQs and BL Lacs) and SED-based classifications (LSP, ISP, and HSP), where, including, 651 FSRQs and 1029 BL Lacs (960 LSP, 334 ISP and 386 HSP). The 1680 blazars are divided into three samples: training, validation, and forecast. Where, the 651 FSRQs and 701 (ISP and HSP) BL Lacs are viewed as the training and validation samples; All 328 LSP BL Lacs are viewed as a forecast sample.

We selected the data from the 4LAC-DR2 table[4] of the 4LAC-DR2 catalog (Lott et al. 2020) and the 4FGL-DR2 table[5] of the 4FGL-DR2 catalog (Ballet

[1] https://www.R-project.org/

[2] https://doi.org/10.48550/arXiv.2010.08406

[3] https://fermi.gsfc.nasa.gov/ssc/data/access/lat/4LACDR2/

[4] https://fermi.gsfc.nasa.gov/ssc/data/access/lat/4LACDR2/table-4LAC-DR2-h.fits

[5] https://fermi.gsfc.nasa.gov/ssc/data/access/lat/10yr_catalog/gll_psc_v27.fit

et al. 2020). The 4LAC-DR2 FITS table ("table-4LAC-DR2-h.fits") lists 37 variables (37 columns). In the 4FGL-DR2 FITS table ("gll_psc_v27.fit") of the 4FGL-DR2 catalog, 74 variables are reported using 142 columns (also see Table 12 of Abdollahi et al. 2020). Among the 74 variables, some variables contain multiple columns. For instance, the parameters: "Flux_Band" with seven columns are used to present the integral photon flux in each of the seven spectral bands that are marked as Flux_Band1, Flux_Band2 ... respectively; "nuFnu_Band" with seven columns are used to present the SED for the spectral bands, marked as nuFnu_Band1, nuFnu_Band2 ... respectively (see Table 1); and so on. For the description of other multi-column parameters can be referenced in Abdollahi et al. (2020) or Kang et al. (2019b).

In addition to all the parameters (data columns) reported in 4FGL-DR2 and 4LAC-DR2, following Ackermann et al. (2012), similar to Doert & Errando (2014) and Saz Parkinson et al. (2016) and Zhu et al. (2021), the hardness ratios are calculated using the following Equation:

$$HR_{ij} = \frac{nuFnu\_Band_j - nuFnu\_Band_i}{nuFnu\_Band_j + nuFnu\_Band_i} \tag{1}$$

where i and j are indices corresponding to the seven different spectral energy bands defined in the 4FGL-DR2 catalog: $i, j = 1$: $50 - 100$MeV; 2: $100 - 300$MeV; 3: 300MeV $-$ 1GeV; 4: $1 - 3$GeV; 5: $3 - 10$GeV; 6: $10 -$ 30GeV; and 7: $30 - 300$ GeV. Combining two hardness ratios, a hardness curvature parameter was also constructed as:

$$HRC_{ijk} = HR_{ij} - HR_{jk} \tag{2}$$

for instance, $\mathrm{HRC}_{234} = \mathrm{HR}_{23}$-$\mathrm{HR}_{34}$, where 2, 3, and 4 are indices for 2: $100 - 300$MeV; 3: 300MeV $-$ 1GeV; 4: $1 - 3$GeV; respectively.

Based on the VLBI counterpart listed in 4LAC-DR2 catalog (see Lott et al. 2020), using the TOPCAT [6] software (Taylor 2005), we cross-matching the latest version ("rfc_2022a", as of May 20, 2022) of the Radio Fundamental Catalog (RFC)[7], which is the most complete catalogue of positions of compact radio sources and list 20,499 sources (see Beasley et al. 2002; Fomalont et al. 2003; Petrov 2021 and references therein). This flux density (unit in Jy) of the S-band, C-band, X-band (F_X), U-band, and K-band are obtained. Among the 1680 selected sources, which match 877 radio data in S-band; 785 radio data in C-band; 1483 radio data in X-band; 374 radio data in U-band; and 337 radio data in K-band. The matching number of the X-band is the largest, which includes 1185 ($\sim$87.66%$\simeq$1185/1352) sources with observational data (still 167 source data missing) in the training and validation sample; 298 ($\sim$90.85% $\simeq$ 298/328) sources with observational data (and still 30 source data missing) in the forecast sample.

Similar to the data sample's parameter selection rules of previous work (see Kang et al. 2019b for the detailed description), firstly, the subset of parameters and their associated data are identified. Where, the coordinate columns, error columns, string columns, and most data missing columns are removed; Keeping one of the same data columns from the 4LAC table and the 4FGL table; Merging the defined data (e.g., "HR_{ij}, HRC_{ijk}") that are created above using equation 1 and 2; And for the VLBI radio data, only the X-band flux density was chosen because there are too many missing data for other bands. The 45 candidate parameters were preliminarily selected (see Table 1) from the 4LAC table, 4FGL table, created data and RFC data.

In order to simplify the calculation, some parameters are pre-selected for the SML algorithms. The Two Sample Kolmogorov-Smirnov test (e.g.,Acuner & Ryde 2018; Kang et al. 2019a,b, 2020) is applied to two subsamples of the data (651 FSRQs and 701 ISP (and HSP) BL Lacs) to calculate the independence of the 45 parameters, the results are summarized in Table 1; Also, the Gini coefficients, which is an established method to determine the variables' importance (see Liaw & Wiener 2002; Breiman 2001 for the details and references therein), are also computed by applying a RF algorithm (see Section 2) to the 45 parameters' data. The results are consistent with those of the two sample K-S tests and are also presented in Table 1. Considering $p > 0.05$[8] and the Gini coefficients (Gini $\simeq$ 0.000), one parameter ("PLEC_Exp_Index") is excluded; Comparing D-values in K-S test and the Gini coefficients in RFs, for the similar or identical parameters (see Table 1), the four parameters with a less D-values and Gini coefficients: LP_Index and PLEC_Index, or PL_Flux_Density, LP_Flux_Density, are also excluded; PL_Index and PLEC_Flux_Density with a bigger D-

[6] http://www.star.bris.ac.uk/~mbt/topcat/

[7] http://astrogeo.org/sol/rfc/rfc_2022a/

[8] where, p > 0.05 indicates that the two populations should be the same distribution, which does not reject the null hypothesis

Table 1. The Results of the Two-sample K-S Test for 651 FSRQs and 701 ISP (and HSP) BL Lacs

Label (1)	Selected Parameters (2)	D of K-S test (3)	p of K-S test (4)	MeanDecreaseGini (5)
1	PL_Index	0.845	<1E-16	82.172
2	$X\_band.$	0.816	<1E-16	64.389
3	$Pivot\_Energy$	0.805	<1E-16	58.089
4	$HR45$	0.708	<1E-16	30.761
5	$PLEC\_Flux\_Density$	0.688	<1E-16	29.138
6	$HR34$	0.658	<1E-16	23.982
7	$HR56$	0.657	<1E-16	21.482
8	$nuFnu\_Band7$	0.600	<1E-16	15.884
9	$Flux\_Band2$	0.562	<1E-16	7.420
10	$Flux\_Band7$	0.564	<1E-16	12.496
11	$nuFnu\_Band2$	0.554	<1E-16	7.354
12	$PLEC\_Expfactor$	0.545	<1E-16	8.531
13	$Frac\_Variability$	0.530	<1E-16	9.742
14	$HR67$	0.504	<1E-16	3.819
15	$Variability\_Index$	0.478	<1E-16	6.189
16	$Flux\_Band3$	0.467	<1E-16	4.192
17	$Npred$	0.460	<1E-16	4.101
18	$nuFnu\_Band3$	0.447	<1E-16	3.190
19	$nuFnu\_Band6$	0.427	<1E-16	8.957
20	$Flux\_Band6$	0.409	<1E-16	5.787
21	$HR23$	0.378	<1E-16	2.136
22	$Flux\_Band1$	0.342	<1E-16	2.294
23	$nuFnu\_Band1$	0.341	<1E-16	2.154
24	$HS123$	0.244	<1E-16	2.165
25	$HS234$	0.247	<1E-16	2.528
26	LP_beta	0.256	<1E-16	2.918
27	$Energy\_Flux100$	0.233	<1E-16	2.378
28	$Flux\_Band4$	0.227	3.33E-16	1.921
29	$LP\_SigCurv$	0.237	<1E-16	2.790
30	$nuFnu\_Band4$	0.212	3.02E-14	2.052
31	$HR12$	0.211	4.46E-14	2.042
32	$PLEC\_SigCurv$	0.208	1.01E-13	2.839
33	$HS345$	0.179	2.46E-10	1.942
34	$HS456$	0.165	8.89E-09	2.466
35	$Flux1000$	0.142	1.23E-06	2.384
36	$nuFnu\_Band5$	0.142	1.28E-06	3.128
37	$Signif\_Avg$	0.121	5.77E-05	2.992
38	$Flux\_Band5$	0.120	6.95E-05	2.362
39	$nuFnu\_syn$	0.121	6.33E-05	3.616
40	$HS567$	0.107	5.62E-04	2.089
41	$PLEC\_Exp\_Index$	0.001	1.00E+00	0.000
42	LP_Index	0.793	<1E-16	52.481
43	$LP\_Flux\_Density$	0.685	<1E-16	21.968
44	$PL\_Flux\_Density$	0.684	<1E-16	24.419
45	$PLEC\_Index$	0.586	<1E-16	10.554

NOTE—Column 1 presents the parameter labels in the sample. Column 2 lists the selected parameters. The two-sample Kolmogorov-Smirnov test results for the test statistic (D) and the p-value(p) are presented in Columns 3 and 4, respectively. The Gini coefficient (Gini), an indicator of variable importance in RFs are presented in Column 5.

values and Gini coefficients are selected. Therefore, 40 parameters are selected in this work.

For the selected 40 parameters, there are 1.099512 E+12 different combinations, which need to costs too long time to utilize the RF to calculate each combination of parameters. This is not possible for us to accomplish. In order to reduce the calculation time, to ensure the study can be completed (see Kang et al. 2019b for the detailed description), we further sub-selected 23 parameters by considering D > 0.300 in the K-S test and Gini > 2.000 in RF algorithm. A simple horizontal line is introduced in the table to distinguish the collection of 23 parameters utilized. Based on the selected 23 parameters, a subset of the data sample is selected from the 4FGL table, 4LAC table, created data and RFC data, which includes 1680 blazars (651 FSRQs, 701 ISP and HSP BL Lacs, and 328 LSP BL Lacs). These 328 LSP BL Lacs are listed in Table 4.

4. OPTIMAL COMBINATIONS OF PARAMETERS AND RESULTS

The selected 1680 blazars are divided into three samples: training, validation, and forecast. Where, the 651 FSRQs and 701 (ISP and HSP) BL Lacs are viewed as the training and validation samples; All 328 LSP BL Lacs are viewed as a forecast sample. Approximately 4/5 of 1352 blazars (651 FSRQs and 701 (ISP and HSP) BL Lacs) are randomly (random seed = 123) assigned to the training sample, and the remaining ones (e.g., approximately 1/5) are considered as the validation sample. Here, the training sample include 1082 blazars (528 FSRQs and 554 ISP, or HSP BL Lacs), and the validation sample has 270 blazars (123 FSRQs and 147 ISP, or HSP BL Lacs).

For the finally sub-selected 23 parameters of 1680 sources, there are 8388607 different combinations. Then, the optimal parameters combinations **(OPC)** are searched based on the training, validation and forecast samples using the RF algorithms. The default settings for the RF classification functions ($randomForest()$ in R code) are used to simplify the calculations. After the predictive models are generated and assessed; an effective predictive model is used to forecast whether a LSP BL Lac belongs to the intrinsically FRSQ or the actually BL Lac class based on its predictor variables. The main steps to accomplish this in the R platform are publicly available[9].

The prediction accuracies of the different parameter combinations in the RF SML algorithms are computed. The highest prediction accuracies for different combinations of parameters in the RF algorithms (represented with a red solid dots + dashed line) are illustrated in Figure 1. As the number of parameters increases, the accuracy gradually reaches its maximum. Here, with 5, 6, 7, 8, 9, 10, 11, 12, or 13 parameters combinations (see Table 2), the accuracy of the RF algorithm reaches its maximum. Where, 178 OPCs in total 8388607 different combinations are hunted. There is 1, 5, 14, 35, 52, 39, 28, 2, or 2 combinations of 5, 6, 7, 8, 9, 10, 11, 12, or 13 parameters achieving a maximum accuracy (accuracy$\simeq$0.9889) respectively. (see Table 2 and 3). When more parameters are applied, the accuracy begins to decline. These results are consistent with the conclusions of our previous work (Kang et al. 2019b).

From the 178 OPCs (see Table 2 and 3), we select nine combinations, here one combination in one of the combinations with 5, 6, 7, 8, 9, 10, 11, 12, or 13 parameters, respectively (see Table 2 for the parameter with underline or marked * in the number of parameters, e.g., 5*). Combined the classification results from the nine OPCs (**C_9 predictions**), 113 actually BL Lac type (**ABLLs**) and 157 possible Changing-Look Blazar Candidates (**CLBCs**) that intrinsically FSRQs misclassified as BL Lacs are predicted; however, 58 remain without a clear prediction, for 328 LSP BL Lacs reported in the high Galactic latitudes ($|b| > 10°$) 4LAC-DR2 catalog. The predicted results of 328 LSP BL Lacs are listed in Table 4.

In the $logF_X$-Γ_{ph} (Fermi γ-ray photon spectral index and the X-band VLBI radio flux) plane for the LSP BL Lacs, we note that the prediction results, between the 113 ABLLs (black dots) and 157 CLBCs (red squares) sources, show a clear separation (see Figure 2). In the two-dimensional parameters space, a simply phenomenological critical line (e.g., $A*x+B*y+C=0$) can is employed to roughly separate these two subclasses (ABLLs and CLBCs) (e.g., see Chen 2018). Which (This criterion/line) can be obtained from the Support Vector Machines (SVM, the function $svm()$ of the e1071 package in R, see Meyer et al. 2021 for details) with kernel = "linear" (other settings with default) in two-dimensional

[9] https://github.com/ksj7924/Kang2022ApJRcode

parameters space. The optimal critical lines (e.g., see equation 3 identified as the dotted-dashed red lines in Figure 2) with the accuracy value: 92.86% are obtained in the $logF_X$-Γ_{ph} plane:

$$3.854992 * \Gamma_{\rm ph} + 3.274545 * logF_X - 5.541661 = 0. \quad (3)$$

Of these, 96 of the 113 ABLL sources (96/113∼84.96%) are in the lower left of the line; 151 of the 157 CLBC sources (151/157∼96.18%) are in the upper right of the line.

Comparing the CLBCs with the ABLLs and the FSRQs reported in 4LAC (green open squares in right panel in Figure 2), we found that the $logF_X$ and Γ_{ph} of the CLBCs source are both slightly larger than that of the ABLLs. The $logF_X$ of the CLBCs and that of the FSRQ are overlapping and cannot be distinguished; However, the photon spectral index of the CLBCs is a little smaller than that of the FSRQ. The CLBC sources are located in the regions where the $logF_X$ is large relative to the ABLL and the the photon spectral index is small relative to the FSRQs. These CLBC sources may be intrinsically FSRQs with broad emission lines, which may be mistaken for BL Lac-type sources due to their strong jet continuum swamping the broad emission lines and showing relatively small EW. When the continuum becomes weaker, the emission lines should exhibit a wider FSRQ-type EWs. These CLBCs may be the candidates for the transition from BL Lac to FSRQ (B-to-F transition), and the region (above line) where the CLBCs are located (see Figure 2) can be referred to as the from BL Lac to FSRQ transition region, named as B-to-F transition region (called as "$B \to F$" zone).

Table 2. The test accuracy, predict results , and parameters for the optimal combinations in RF algorithm.

N	N_{bll}	N_{fsrq}	Acc	p1	p2	p3	p4	p5	p6	p7	p8	p9	p10	p11	p12	p13
(1)	(2)	(3)	(4)	(5)	(6)	(7)	(8)	(9)	(10)	(11)	(12)	(13)	(14)	(15)	(16)	(17)
5*	137	191	0.9889	2	4	5	7	13	...	...	...	...	...	...	...	...
6*	138	190	0.9889	2	4	7	8	18	19	...	...	...	...	...	...	...
6	140	188	0.9889	2	4	5	7	13	18	...	...	...	...	...	...	...
6	141	187	0.9889	2	4	5	7	13	20	...	...	...	...	...	...	...
6	139	189	0.9889	2	4	5	12	13	19	...	...	...	...	...	...	...
6	140	188	0.9889	2	4	8	13	16	19	...	...	...	...	...	...	...
7*	140	188	0.9889	2	4	5	7	9	13	18	...	...	...	...	...	...
7	141	187	0.9889	2	4	5	7	12	13	15	...	...	...	...	...	...
7	142	186	0.9889	2	4	5	7	12	13	19	...	...	...	...	...	...
7	143	185	0.9889	2	4	5	7	12	13	20	...	...	...	...	...	...
7	137	191	0.9889	2	4	5	7	13	15	17	...	...	...	...	...	...
7	138	190	0.9889	2	4	5	7	13	15	18	...	...	...	...	...	...
7	139	189	0.9889	2	4	5	7	13	15	19	...	...	...	...	...	...
7	142	186	0.9889	2	4	5	7	13	15	20	...	...	...	...	...	...
7	141	187	0.9889	2	4	5	7	13	16	18	...	...	...	...	...	...
7	143	185	0.9889	2	4	5	7	13	16	19	...	...	...	...	...	...
7	139	189	0.9889	2	4	5	7	13	20	22	...	...	...	...	...	...
7	128	200	0.9889	2	8	10	13	14	18	19	...	...	...	...	...	...
7	141	187	0.9889	2	4	8	13	14	19	21	...	...	...	...	...	...
7	138	190	0.9889	2	4	8	13	14	20	23	...	...	...	...	...	...
8*	146	182	0.9889	2	4	7	8	13	18	19	20	...	...	...	...	...
8	142	186	0.9889	2	4	5	7	8	13	14	19	...	...	...	...	...

Table 2 *continued*

Table 2 *(continued)*

N	N_{bll}	N_{fsrq}	Acc	p1	p2	p3	p4	p5	p6	p7	p8	p9	p10	p11	p12	p13
(1)	(2)	(3)	(4)	(5)	(6)	(7)	(8)	(9)	(10)	(11)	(12)	(13)	(14)	(15)	(16)	(17)
8	140	188	0.9889	2	4	5	7	9	12	13	19	...	...	...	...	...
8	137	191	0.9889	2	4	5	7	9	12	13	20	...	...	...	...	...
8	141	187	0.9889	2	4	5	7	9	13	18	23	...	...	...	...	...
8	141	187	0.9889	2	4	5	7	11	12	13	20	...	...	...	...	...
8	140	188	0.9889	2	4	5	7	11	13	16	22	...	...	...	...	...
8	143	185	0.9889	2	4	5	7	12	13	14	19	...	...	...	...	...
8	143	185	0.9889	2	4	5	7	12	13	14	20	...	...	...	...	...
8	140	188	0.9889	2	4	5	7	12	13	15	19	...	...	...	...	...
8	141	187	0.9889	2	4	5	7	12	13	15	20	...	...	...	...	...
8	143	185	0.9889	2	4	5	7	12	13	16	20	...	...	...	...	...
8	144	184	0.9889	2	4	5	7	12	13	17	19	...	...	...	...	...
9^{*}	136	192	0.9889	2	4	6	8	12	13	14	19	20	...	...	...	...
10^{*}	139	189	0.9889	2	4	5	7	8	12	13	15	19	22	...	...	...
11^{*}	136	192	0.9889	2	4	7	8	9	10	13	14	19	20	22	...	...
12^{*}	143	185	0.9889	2	4	5	7	12	13	15	18	19	20	21	22	...
13^{*}	144	184	0.9889	2	4	5	7	8	12	13	14	15	19	20	21	22
...	...	...	...	...	...	...	...	...	...	...	...	...	...	...	...	...

Note—The number of parameters for the optimal combination are presented in Column 1. The highest accuracies of each classifier are presented in Column 4. The number of BL Lacs (ABLLs) and FSRQs (CLBCs) predicted by Random Forests algorithm with the default settings for the LSP BL Lacs (predicted dataset) are presented in Columns 2 and 3. The labels of the parameters are presented in Columns 5-17, these correspond to the labels in Table 1, Column 1. Here, the one combination for the different number of parameters for the optimal combinations is shown for guidance regarding its form and content.

(This table is available in its entirety in machine-readable form.)

Table 3. The Number of the Optimal Parameters and Combinations

Algorithm	5 Par	6 Par	7 Par	8 Par	9 Par	10 Par	11 Par	12 Par	13 Par
(1)	(2)	(3)	(4)	(5)	(6)	(7)	(8)	(9)	(10)
RFs	1	5	14	35	52	39	28	2	2

Note—The Algorithm are presented in Column 1. The number of combinations with the highest accuracies in RFs algorithm for 5−13 parameters are presented in Columns 2−10 (see the machine-readable format of Table 2 for the details).

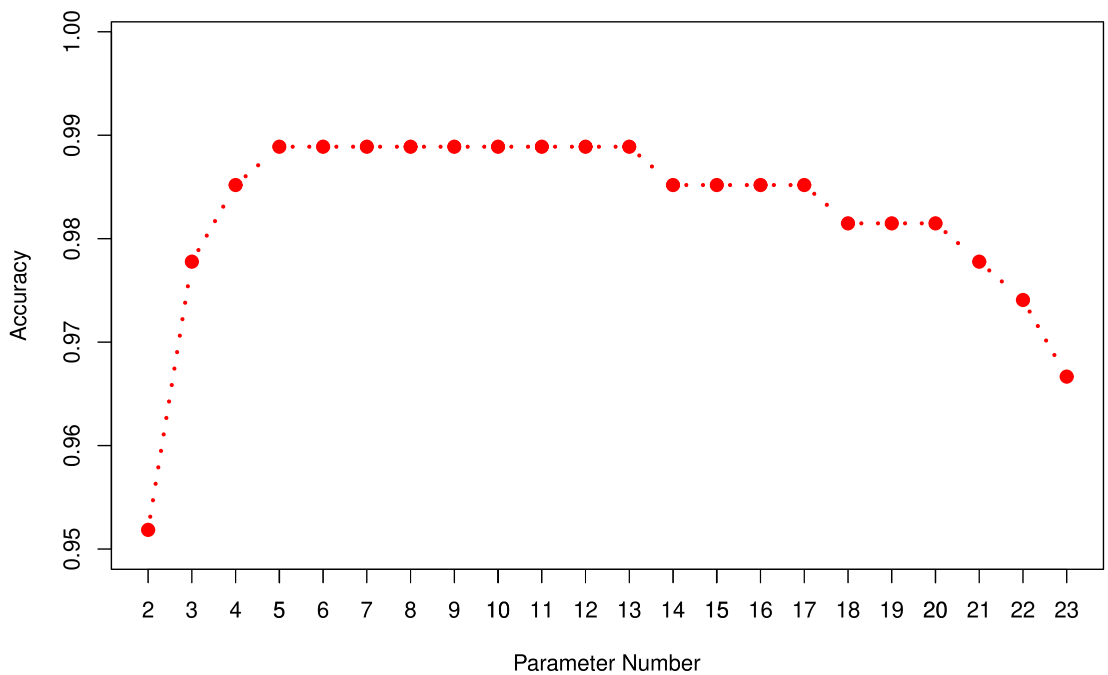

Figure 1. Highest accuracy for the different number of combinations of parameters in Random Forests algorithm.

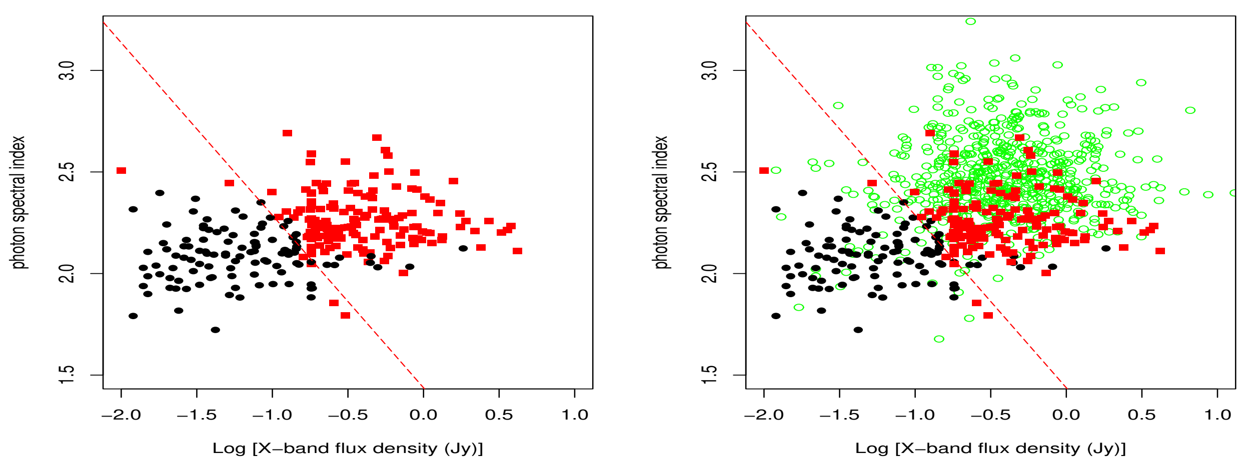

Figure 2. Classification scatterplots for the Fermi γ-ray photon spectral index (Γ_{PH}) and the X-band VLBI radio flux (log F_X), where the black filled circles, red solid squares, and green empty circles indicate ABLLs, CLBCs and FSRQ respectively.

Table 4. The predicted classification results of Fermi LSP BL Lacs

4FGL name	ASSOC_3FGL	RF5	RF6	RF7	RF8	RF9	RF10	RF11	RF12	RF13	C_9	M_{Fan}	M_{CKZ}	CD
(1)	(2)	(3)	(4)	(5)	(6)	(7)	(8)	(9)	(10)	(11)	(12)	(13)	(14)	(15)
4FGL J0001.2−0747	3FGL J0001.2−0748	fsrq	fsrq	fsrq	bll	bll	fsrq	fsrq	fsrq	bll	UNK	...	...	...
4FGL J0003.2+2207		bll	bll	bll	bll	bll	bll	fsrq	bll	bll	UNK	...	...	...
4FGL J0003.9−1149	3FGL J0003.8−1151	fsrq	fsrq	fsrq	fsrq	fsrq	fsrq	fsrq	fsrq	fsrq	FSRQ	...	...	...
4FGL J0006.3−0620		fsrq	fsrq	fsrq	fsrq	fsrq	fsrq	fsrq	fsrq	fsrq	FSRQ	...	...	...
4FGL J0008.0+4711	3FGL J0008.0+4713	bll	bll	bll	bll	bll	bll	bll	bll	bll	BLL	...	...	...
4FGL J0009.1+0628	3FGL J0009.1+0630	bll	bll	bll	bll	bll	bll	bll	bll	bll	BLL	...	...	...
4FGL J0013.1−3955	3FGL J0013.2−3954	fsrq	fsrq	fsrq	fsrq	fsrq	fsrq	fsrq	fsrq	fsrq	FSRQ	...	...	...
4FGL J0014.1+1910	2FGL J0013.8+1907	fsrq	fsrq	fsrq	fsrq	fsrq	fsrq	fsrq	fsrq	fsrq	FSRQ	...	...	1.41
4FGL J0019.6+2022	3FGL J0019.4+2021	fsrq	fsrq	fsrq	fsrq	fsrq	fsrq	fsrq	fsrq	fsrq	FSRQ	...	...	...
4FGL J0022.1−1854	3FGL J0022.1−1855	bll	bll	bll	bll	bll	bll	bll	bll	bll	BLL	...	...	...
4FGL J0022.5+0608	3FGL J0022.5+0608	bll	fsrq	bll	fsrq	fsrq	fsrq	fsrq	bll	fsrq	UNK	...	...	...
4FGL J0023.9+1603		bll	bll	bll	bll	bll	bll	bll	bll	bll	BLL	...	...	...
4FGL J0029.0−7044	3FGL J0029.1−7045	fsrq	fsrq	fsrq	bll	bll	fsrq	fsrq	bll	fsrq	UNK	...	...	...
4FGL J0032.4−2849	3FGL J0032.3−2852	bll	fsrq	bll	fsrq	fsrq	fsrq	bll	fsrq	fsrq	UNK	...	...	1.26
4FGL J0035.8−0837		bll	bll	bll	bll	bll	bll	bll	bll	bll	BLL	...	...	...
4FGL J0038.1+0012	3FGL J0038.0+0012	bll	bll	bll	bll	bll	bll	bll	bll	bll	BLL	...	...	...
4FGL J0040.3+4050	3FGL J0040.3+4049	bll	bll	bll	bll	bll	bll	bll	bll	bll	BLL	...	...	...
4FGL J0049.7+0237	3FGL J0049.7+0237	fsrq	fsrq	fsrq	fsrq	fsrq	fsrq	fsrq	fsrq	fsrq	FSRQ	Fan_fsrq	...	...
4FGL J0056.8+1626		fsrq	fsrq	fsrq	fsrq	fsrq	fsrq	fsrq	fsrq	fsrq	FSRQ	...	...	...
4FGL J0058.0−3233	3FGL J0058.0−3233	bll	bll	bll	bll	bll	bll	bll	bll	bll	BLL	...	...	...
4FGL J0105.1+3929	3FGL J0105.3+3928	fsrq	fsrq	fsrq	fsrq	fsrq	fsrq	fsrq	fsrq	fsrq	FSRQ	...	...	1.95
4FGL J0107.4+0334		fsrq	fsrq	fsrq	fsrq	fsrq	fsrq	fsrq	fsrq	fsrq	FSRQ	...	...	...
4FGL J0112.1+2245	3FGL J0112.1+2245	bll	bll	bll	bll	bll	bll	bll	bll	bll	BLL	...	...	...
4FGL J0113.7+0225		fsrq	fsrq	fsrq	fsrq	fsrq	fsrq	fsrq	fsrq	fsrq	FSRQ	...	...	...
4FGL J0124.8−0625	3FGL J0125.2−0627	fsrq	bll	fsrq	fsrq	fsrq	fsrq	fsrq	fsrq	fsrq	UNK	...	...	...
4FGL J0125.3−2548	3FGL J0125.4−2548	fsrq	fsrq	fsrq	fsrq	fsrq	fsrq	fsrq	fsrq	fsrq	FSRQ	...	...	...
4FGL J0127.2−0819	3FGL J0127.1−0818	bll	bll	bll	bll	bll	bll	bll	bll	bll	BLL	...	...	...

Table 4 *continued*

Table 4 *(continued)*

4FGL name (1)	ASSOC_3FGL (2)	RF5 (3)	RF6 (4)	RF7 (5)	RF8 (6)	RF9 (7)	RF10 (8)	RF11 (9)	RF12 (10)	RF13 (11)	C_9 (12)	M_{Fan} (13)	M_{CKZ} (14)	CD (15)
4FGL J0141.4−0928	3FGL J0141.4−0929	fsrq	fsrq	fsrq	fsrq	fsrq	fsrq	fsrq	fsrq	fsrq	FSRQ	Fan_fsrq	...	...
4FGL J0142.7−0543		bll	bll	bll	fsrq	fsrq	bll	fsrq	bll	bll	UNK	...	...	...
4FGL J0144.6+2705	3FGL J0144.6+2705	fsrq	fsrq	fsrq	fsrq	fsrq	fsrq	fsrq	fsrq	fsrq	FSRQ	...	...	...
4FGL J0148.6+0127	3FGL J0148.6+0128	bll	bll	bll	bll	bll	bll	bll	bll	bll	BLL	...	...	...
4FGL J0202.7+4204	3FGL J0202.5+4206	fsrq	fsrq	fsrq	fsrq	fsrq	fsrq	fsrq	fsrq	fsrq	FSRQ	...	...	...
4FGL J0203.6+7233	3FGL J0204.0+7234	fsrq	fsrq	fsrq	fsrq	fsrq	fsrq	fsrq	fsrq	fsrq	FSRQ	...	...	...
4FGL J0203.7+3042	3FGL J0203.6+3043	fsrq	fsrq	fsrq	fsrq	fsrq	fsrq	fsrq	fsrq	fsrq	FSRQ	...	...	2.34
4FGL J0208.3−6838	3FGL J0208.0−6838	bll	bll	bll	bll	bll	bll	bll	bll	bll	BLL	...	...	...
4FGL J0208.5−0046		fsrq	fsrq	fsrq	fsrq	fsrq	fsrq	fsrq	fsrq	fsrq	FSRQ	...	...	...
4FGL J0209.9+7229		fsrq	fsrq	fsrq	fsrq	fsrq	fsrq	fsrq	fsrq	fsrq	FSRQ	...	CKZ_fsrq	2.24
4FGL J0217.2+0837	3FGL J0217.2+0837	fsrq	fsrq	fsrq	fsrq	fsrq	fsrq	fsrq	fsrq	fsrq	FSRQ	...	...	...
4FGL J0219.5+0724		bll	bll	bll	bll	bll	bll	bll	bll	bll	BLL	...	...	...
4FGL J0224.0−7941	3FGL J0224.1−7941	fsrq	fsrq	fsrq	fsrq	fsrq	fsrq	fsrq	fsrq	bll	UNK	...	...	...
4FGL J0231.2−5754	3FGL J0230.6−5757	bll	bll	bll	bll	bll	bll	bll	bll	bll	BLL	...	...	...
4FGL J0238.6+1637	3FGL J0238.6+1636	fsrq	fsrq	fsrq	fsrq	fsrq	fsrq	fsrq	fsrq	fsrq	FSRQ	Fan_fsrq	...	2.69
4FGL J0241.0−0505		bll	fsrq	bll	bll	fsrq	bll	bll	bll	bll	UNK	...	...	...
4FGL J0243.4+7119	3FGL J0243.5+7119	bll	bll	bll	bll	bll	bll	bll	bll	bll	BLL	...	...	...
4FGL J0245.1−0257		bll	bll	bll	bll	bll	bll	bll	bll	bll	BLL	...	...	...
4FGL J0359.4−2616	3FGL J0359.3−2612	fsrq	fsrq	fsrq	fsrq	fsrq	fsrq	fsrq	fsrq	fsrq	FSRQ	...	CKZ_fsrq	...
4FGL J0402.0−2616	3FGL J0402.1−2618	bll	bll	bll	bll	bll	bll	bll	bll	bll	BLL	...	...	...
4FGL J0403.5−2437	3FGL J0403.7−2442	fsrq	fsrq	fsrq	fsrq	fsrq	fsrq	fsrq	fsrq	fsrq	FSRQ	...	CKZ_fsrq	...
4FGL J0407.5+0741	3FGL J0407.5+0740	fsrq	fsrq	fsrq	fsrq	fsrq	fsrq	fsrq	fsrq	fsrq	FSRQ	Fan_fsrq	CKZ_fsrq	2.69
...	...	...	...	...	...	...	...	...	...	...	...	...	...	...

NOTE—The 4FGL names are listed in Column 1 and the counterpart names of the previous 3FGL source catalogs are presented in Column 2. The predicted classification results using RF algorithm for the different parameter combinations in the work are shown in columns 3-11. The combined classification results (C_9 predictions) is presented in Column 12. Column 13 and 14 list the predicted classification results (M_{Fan}) in Fan & Wu (2019) and (M_{CKZ}) in Cheng et al. (2022), respectively. The CD values reported in Paliya et al. (2021) are listed in Column 15. Table 4 is published in its entirety in the machine-readable format. A portion is shown here for guidance regarding its form and content.

(This table is available in its entirety in machine-readable form.)

Table 5. Comparison of the other work's Predictions.

Algorithm	Class	RF Predictions	Fan Predictions	CKZ Predictions	CKZ Predictions	Paliya Predictions
(1)	(2)	(3)	(4)	(5)	(6)	(7)
	N	328	33 FSRQs	47 FSRQs	39 FSRQs	626 CD > 1
	M	328	29	39	31	33
	FSRQ	157	24	38	30	22
RF	BLL	113	2	...	...	5
	UNK	58	3	1	1	6

Note—The classifiers and classes are presented in Column 1 and 2. Columns 3 lists the results of RF Predictions in the work. Columns 4-7 presents the results of comparison of the Fan's predictions in Fan & Wu (2019); the CKZ's predictions in Cheng et al. (2022) (where, Columns 6 lists the sources have CD) ; the Paliya's Predictions in Paliya et al. (2021) for common objects. Where, N is the number of the Fan's predictions, CKZ's predictions and Paliya's Predictions; M shows the number of RF Predictions of the work in the cross-matching the FAN's predictions, CKZ's predictions and Paliya's Predictions.

5. RESULTS COMPARISON

Cross-matching the C_9 predictions (CLBCs) and the predictions of Fan & Wu (2019), of the 33 LSP BL Lac sources predicted as the possible FSRQ style sources by Fan & Wu (2019), there are 29 sources in our sample. Among the 29 possible FSRQ style sources predicted by Fan & Wu (2019), the prediction results of 24 sources in the work are consistent with the prediction results of Fan & Wu (2019); However, our predictions for 3 sources (4FGL J0428.6-3756; 4FGL J0811.4+0146 and 4FGL J0818.2+4222) are remain no clear prediction; there are 2 sources (4FGL J0433.6+2905 and 4FGL J0738.1+1742) that are predicted as BL Lacs in our work (see Table 4 and Table 5).

In Paliya et al. (2021), the Compton dominance (CD; the ratio of the inverse Compton to synchrotron peak luminosities) for 1030 Fermi blazars are calculated. They found that the CD and accretion luminosity (L_{disk}) in Eddington units (L_{disk}/L_{Edd}) are positively correlated, suggesting that the CD can be used to reveal the state of accretion in blazars and used to distinguish the classification of blazars. They suggest that blazars with CD $>$ 1 should be identified as FSRQs and CD $<$1 as BL Lac objects. There are 626 blazars with CD $>$ 1 in their sample. Cross-matching the C_9 prediction results and the 626 blazars identified as FSRQs in Paliya et al. (2021), we obtained 33 common sources. Among the 33 common objects, 22 FSRQ candidates are consistent between our predictions and Paliya et al. (2021) predictions (see Table 4 and Table 5). 5 ABLLs (4FGL J0433.6+2905; 4FGL J1008.8-3139; 4FGL J1035.6+4409; 4FGL J1503.5+4759 and 4FGL J1942.8-3512) and 6 UNKs (4FGL J0032.4-2849 ; 4FGL J0428.6-3756; 4FGL J0811.4+0146; 4FGL J1331.2-1325; 4FGL J1647.5+4950 and 4FGL J1704.2+1234) were predicted in our predictions.

When, cross-matching the C_9 predictions and the prediction results of Cheng et al. (2022), of the 47 LSP BL Lac sources predicted as FSRQ, 39 sources are in our sample. The remaining 8 sources locate in the low Galactic latitudes ($|b| < 10°$) 4LAC-DR2 catalog. Among the 39 sources, the prediction results of 38 sources are consistent with our prediction results; There is only one source (4FGL J2241.2+4120) that does not have a clear prediction in our predictions (see Table 4 and Table 5). In Cheng et al. (2022), they also check the CD of 39 sources based on SEDs fitting using a quadratic polynomial. For the 39 sources (see Columns 6 in Table 5) reported the CD in Cheng et al. (2022), 31 sources are in our sample, the other remaining 8 sources locate in the low Galactic latitudes ($|b| < 10°$) 4LAC-DR2 catalog. There are 30 sources' prediction are consistent with our predictions, in which 28 sources with CD $>$ 1; two sources with CD $<$ 1; One source (4FGL J2241.2+4120 with CD $\simeq$3.689) that does not have a clear prediction in our work; As mentioned above, a comparison of these predictions suggests that our predictions may be promising and valuable.

In Ajello et al. (2020), they found that the $\nu_{\rm p}^{\rm S}$ distributions are overlap between LSP BL Lacs and FSRQs,

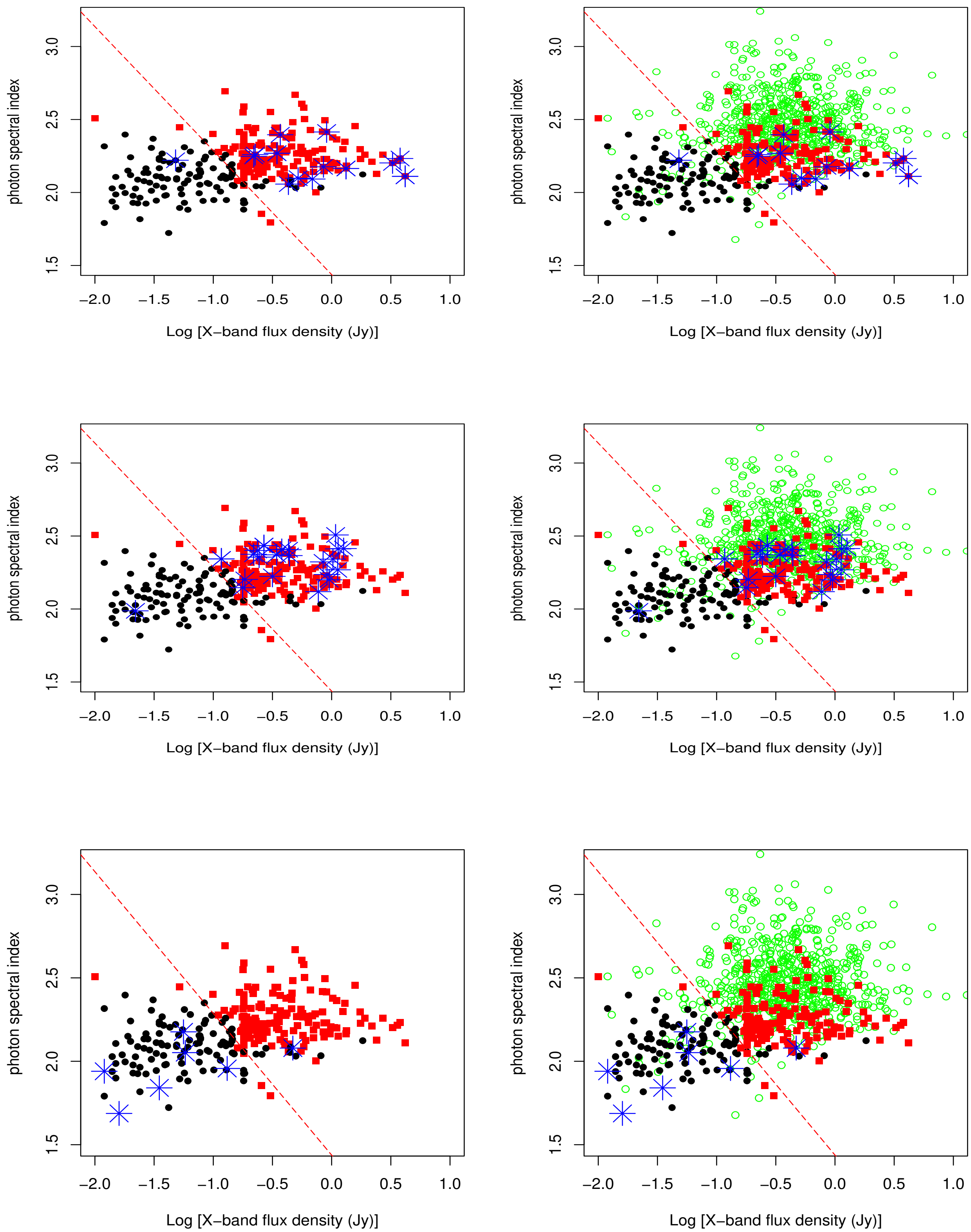

Figure 3. Classification scatterplots for the Fermi γ-ray photon spectral index (Γ_{PH}) and the X-band VLBI radio flux (log F_X), where the black filled circles, red solid squares, and green empty circles indicate ABLLs, CLBCs and FSRQ respectively. And the blue stars represent the LSP BL Lac type (upper panels), the LSP FSRQ type (middle panels), and the HSP and ISP BL Lac type (lower panels), Changing-Look (Transition) Blazars identified in references respectively.

and the gamma-ray photon spectral index (Γ_{ph}) distributions are also very similar. They proposed that there is a possible region for objects that might be transitioning between FSRQs and B L Lacs. There are five of six such transitioning objects found by Ruan et al. (2014) are the LSP subclass reported in 4LAC. In addition, Pei et al. (2022) also address a similar area, based on disk luminosity (L_{disk}) in Eddington units (L_{disk}/L_{Edd}). They propose that there is region (called "appareling zone") with $2.00 \times 10^{-4} \lesssim L_{disk}/L_{Edd} \gtrsim 8.51 \times 10^{-3}$, where, some sources (that are perhaps changing-look blazars) may be a transition between BL Lacs and FSRQs. And they found five confirmed changing-look sources reside in the "appareling" zone.

In the work, a B-to-F transition zone (transition from BL Lac to FSRQ) is suggested by comparing the prediction results: ABLLs and CLBCs. In order to test the effectiveness of the B-to-F zone, we collected a subset of possible, confirmed CLB sources or transition sources (**TCLBs**) and compiled them into An online Changing-Look (Transition) Blazars Catalog (CLB Catalog[10], https://github.com/ksj7924/CLBCat) (**Kang et al., in preparation, also see Appendix A for a part of content.**) presented in https://github.com/ for easy communication. Cross-matching the CLB catalog with our sample, we obtained 49 records from 44 sources with 5 source repeats from some references (e.g., Vermeulen et al. 1995; Corbett et al. 1996; Ghisellini et al. 2011; Shaw et al. 2012; Cutini et al. 2014; Ruan et al. 2014; Padovani et al. 2019; Foschini et al. 2021; Mishra et al. 2021; Peña-Herazo et al. 2021a; Pei et al. 2022). For comparison purposes, all 49 records are listed in Table 6. The 5 sources are 4FGL J0058.4+3315 (reported in Ghisellini et al. 2011 and Shaw et al. 2012); 4FGL J0238.6+1637 and 4FGL J0538.8−4405 (Ghisellini et al. 2011 and Pei et al. 2022); 4FGL J0833.9+4223 (Ruan et al. 2014 and Foschini et al. 2021); and 4FGL J1001.1+2911(Shaw et al. 2012 and Peña-Herazo et al. 2021a), respectively.

We note that all the five of six transitioning objects found by Ruan et al. (2014) are in our sample. Two BL Lac type TCLBs (sources): 4FGL J1250.6+0217 (PKS1247+025) and 4FGL J2206.8−0032 (PMN J2206−0031) in our predictions sample. Both of them are predicted as the possible FSRQ type Candidates (CLBC sources); Other 3 FSRQ type TCLBs: 4FGL J0833.9+4223 (OJ 451), 4FGL J1016.0+0512 (TXS1013+054) and 4FGL J1308.5 +3547 (5C 12.291) that are listed in our train sample. The five transitioning objects are shown in Table 6, all of which locate in the B-to-F transition zone.

In Peña-Herazo et al. (2021a), they reported 26 Changing-Look (transitional) blazars (TCLBs). There are 12 TCLBs matched in our sample. 2 LSP BL Lac type TCLBs: one (4FGL J1001.1+2911) is located in the B-to-F transition zone; another (4FGL J1503.5+4759) is not, respectively. And 4 LSP FSRQ type TCLBs are all locate in the B-to-F transition zone. However, the remaining 6 HSP (or ISP) BL Lac type TCLBs are not in the B-to-F transition zone (see Table 6).

There are six BL Lacs reclassified as FSRQs in Ghisellini et al. (2011) based on the BLR luminosity in Eddington units. All of the six sources are in our sample. The four of them are LSP BL Lac type TCLBs; two of six are LSP FSRQ (labeled in 4LAC-DR2) type TCLBs. The two of four LSP BL Lac type TCLBs (4FGL J0238.6+1637 and 4FGL J0538.8−4405) are also reported in Pei et al. (2022) and also suggested that are potential changing-look blazars (from BL Lac to FSRQ). All of them are located in the B-to-F transition zone.

Foschini et al. (2021) compiled a gamma-ray jetted AGN sample based on the 4FGL catalog. They reported 11 changing-look AGNs, 9 of them are blazars labeled as FSRQ in 4FGL catalog, based on a featureless spectrum reported in the previous literature (see Foschini et al. 2021 for more details and references therein). All the 9 FSRQs type TCLBs are in our sample. There are 8 FSRQ type TCLBs are LSP subclass located in the B-to-F transition zone; But, one source: 4FGL J0134.5+2637 labeled as HSP FSRQ in 4FGL catalog that do not locate in the B-to-F transition zone.

In Shaw et al. (2012), they suggested 11 sources are transitional between the standard FSRQs and BL Lac types. Six sources with the low continuum shown as nominal FSRQs and five sources with the very high S/N broad lines analyzed along with the FSRQ. All the 11 sources that are listed in our sample. There are 4 sources labeled as LSP FSRQ in 4LAC-DR2 catalog located the B-to-F transition zone. There are 6 sources labeled as LSP BL Lac in 4LAC-DR2 catalog also located the B-to-F transition zone. However, the remaining one source: 4FGL J0430.3−2507 labeled as ISP BL Lac in 4LAC-DR2 catalog that locate in the Non-B-F transition zone.

The source: 4FGL J1422.3+3223 (B2 1420+326) labeled as LSP FSRQ in 4LAC-DR2 catalog that was

[10] https://github.com/ksj7924/CLBCat

identified as a CLB (changing-look blazar) by Mishra et al. (2021) based on the multi-wavelength photometric and spectroscopic monitoring observations. The source: 4FGL J1153.4+4931 labeled as LSP FSRQ in 4LAC-DR2 catalog that was suggested as changing-look source by Cutini et al. (2014) based on studying the multi-wavelength SEDs, where during GeV gamma-ray flares, the synchronous peak frequencies vary by about two orders of magnitude and anomalous softening X-ray SED. The source: 4FGL J0509.4+0542 (TXS 0506+056, a neutrino source) labeled as LSP BL Lac in 4LAC-DR2 catalog should be reclassified as an FSRQ by Padovani et al. (2019) based on its Eddington ratio, the criterion proposed in Ghisellini et al. (2011) of the BLR luminosity in Eddington units. All these are listed in Table 6. The eponymous/namesake BL Lacertae object, even, the 4FGL J2202.7+4216 (BL Lac), BL Lac itself, the prototype of the class, the prototype of its blazar subclass, is also listed in Table 6. Which show the EW of the emission lines larger than the 5 Å, during a particularly low state (Vermeulen et al. 1995; Corbett et al. 1996; Capetti et al. 2010), ect.

For ease of comparison, the classification scatterplots for the Fermi γ-ray photon spectral index (Γ_{PH}) and the X-band VLBI radio flux ($\log F_X$) are plotted in Figure 3, where the black filled circles, red solid squares, and green empty circles indicate ABLLs, CLBCs predicted in this work and FSRQs labeled in 4FGL, respectively. And the blue stars represent the LSP BL Lac type (upper panels), the LSP FSRQ type (middle panels), and the HSP and ISP BL Lac type (lower panels), Changing-Look (Transition) Blazars identified in references, respectively. The left panels represent the correlation between Γ_{PH} and $\log F_X$ of the ABLLs and CLBCs predicted in this work and CLBs identified in references; In the right panels, the FSRQs labeled in 4FGL are also added (see, green circle).

In the upper panels, for the LSP BL Lac type Changing-Look (Transition) Blazars (TCLB,17 records for 14 sources in Table 6) identified in references (marked as blue stars), we note that most of the TCLB sources (13 sources) are located in the B-to-F transition region. Only one source, 4FGL J1503.5+4759, which is not located in the B-to-F transition region. Similar to LSP BL Lac type TCLBs, most of the FSRQ type TCLBs (24 records for 22 sources) are also located in the B-to-F transition region, where the FSRQ type TCLBs is that the LSP BL Lacs that may have transitioned. one source, 4FGL J0134.5+2637, but it is a HSP FSRQ, which is not located in the B-to-F transition region (see the middle panels in Figure 3). For the entire LSP blazar type TCLBs subclass, there are 40 records for 35 sources (17 records for 14 BL Lacs and 23 records for 21 FSRQs). 39 records for 34 sources are located in the B-to-F transition region. Only one source, 4FGL J1503.5+4759 with $\Gamma_{PH} = 2.221$, and $\log F_X = -1.319$, which is not located in the B-to-F transition region. Which suggested the B-to-F transition region is valid for LSP BL Lac.

However, for the HSP and ISP BL Lac type TCLBs (see, lower panels), Six of 8 sources are not located in the B-to-F transition region, where one source without radio data (see Table 6), one source : 4FGL J0509.4+0542 (TXS 0506+056, a neutrino source) is located in the B-to-F transition region. The results further show that the B-to-F transition region is only valid for the LSP BL Lac subclass, but not for the HSP(ISP) BL Lac subclass.

Table 6. The Changing-Look (transition) blazars reported in reference in our sample

N	4FGL name	Class	SED class	Γ_{PH}	$\log F_X$	references
(1)	(2)	(3)	(4)	(5)	(6)	(7)
1	4FGL J0238.6+1637	bll	LSP	2.165	0.121	Pei2022
2	4FGL J0538.8−4405	bll	LSP	2.111	0.621	Pei2022
3	4FGL J2206.8−0032	bll	LSP	2.247	-0.658	Ruan et al. (2014)
4	4FGL J1250.6+0217	bll	LSP	2.057	-0.366	Ruan et al. (2014)
5	4FGL J0538.8−4405	bll	LSP	2.111	0.621	Ghisellini et al. (2011)
6	4FGL J0811.4+0146	bll	LSP	2.092	-0.163	Ghisellini et al. (2011)
7	4FGL J0238.6+1637	bll	LSP	2.165	0.121	Ghisellini et al. (2011)

Table 6 *continued*

Table 6 *(continued)*

N	4FGL name	Class	SED class	Γ_{PH}	logF_X	references
(1)	(2)	(3)	(4)	(5)	(6)	(7)
8	4FGL J0428.6−3756	bll	LSP	2.098	-0.283	Ghisellini et al. (2011)
9	4FGL J1503.5+4759	bll	LSP	2.221	-1.319	Pena-Herazo et al. (2021)
10	4FGL J1001.1+2911	bll	LSP	2.269	-0.462	Pena-Herazo et al. (2021)
11	4FGL J2202.7+4216	bll	LSP	2.202	0.515	Vermeulen et al. 1995
12	4FGL J1001.1+2911	bll	LSP	2.269	-0.462	Shaw et al. 2012
13	4FGL J1607.0+1550	bll	LSP	2.259	-0.646	Shaw et al. 2012
14	4FGL J2032.0+1219	bll	LSP	2.414	-0.042	Shaw et al. 2012
15	4FGL J0516.7−6207	bll	LSP	2.176	-0.069	Shaw et al. 2012
16	4FGL J1058.4+0133	bll	LSP	2.233	0.578	Shaw et al. 2012
17	4FGL J2315.6−5018	bll	LSP	2.395	-0.434	Shaw et al. 2012
18	4FGL J0833.9+4223	fsrq	LSP	2.434	-0.572	Ruan et al. (2014)
19	4FGL J1016.0+0512	fsrq	LSP	2.223	-0.500	Ruan et al. (2014)
20	4FGL J1308.5+3547	fsrq	LSP	2.366	-0.357	Ruan et al. (2014)
21	4FGL J0058.4+3315	fsrq	LSP	2.343	-0.932	Ghisellini et al. (2011)
22	4FGL J0210.7−5101	fsrq	LSP	2.342	0.011	Ghisellini et al. (2011)
23	4FGL J1043.2+2408	fsrq	LSP	2.323	-0.072	Pena-Herazo et al. (2021)
24	4FGL J1106.0+2813	fsrq	LSP	2.375	-0.660	Pena-Herazo et al. (2021)
25	4FGL J1321.1+2216	fsrq	LSP	2.371	-0.465	Pena-Herazo et al. (2021)
26	4FGL J1512.2+0202	fsrq	LSP	2.146	-0.752	Pena-Herazo et al. (2021)
27	4FGL J0134.5+2637	fsrq	HSP	1.987	-1.658	Foschini, Luigi 2021
28	4FGL J0510.0+1800	fsrq	LSP	2.200	-0.021	Foschini, Luigi 2021
29	4FGL J0449.1+1121	fsrq	LSP	2.507	0.033	Foschini, Luigi 2021
30	4FGL J0719.3+3307	fsrq	LSP	2.203	-0.733	Foschini, Luigi 2021
31	4FGL J1124.0+2336	fsrq	LSP	2.406	-0.365	Foschini, Luigi 2021
32	4FGL J0833.9+4223	fsrq	LSP	2.434	-0.572	Foschini, Luigi 2021
33	4FGL J0509.4+1012	fsrq	LSP	2.408	-0.421	Foschini, Luigi 2021
34	4FGL J0217.8+0144	fsrq	LSP	2.236	-0.039	Foschini, Luigi 2021
35	4FGL J1037.4−2933	fsrq	LSP	2.414	0.101	Foschini, Luigi 2021
36	4FGL J1422.3+3223	fsrq	LSP	2.401	-0.627	Mishra et al. (2021)
37	4FGL J1153.4+4931	fsrq	LSP	2.412	0.055	Cutini et al. (2014)
38	4FGL J0058.4+3315	fsrq	LSP	2.343	-0.932	Shaw et al. 2012
39	4FGL J0923.5+4125	fsrq	LSP	2.355	-0.613	Shaw et al. 2012
40	4FGL J2244.2+4057	fsrq	LSP	2.119	-0.112	Shaw et al. 2012
41	4FGL J2236.3+2828	fsrq	LSP	2.268	0.051	Shaw et al. 2012
42	4FGL J0022.0+0006	bll	HSP	1.533	...	Pena-Herazo et al. (2021)
43	4FGL J0303.3+0555	bll	HSP	1.687	-1.796	Pena-Herazo et al. (2021)
44	4FGL J0916.7+5238	bll	HSP	1.841	-1.456	Pena-Herazo et al. (2021)
45	4FGL J1326.1+1232	bll	HSP	1.940	-1.921	Pena-Herazo et al. (2021)
46	4FGL J1402.6+1600	bll	ISP	1.957	-0.883	Pena-Herazo et al. (2021)
47	4FGL J1730.8+3715	bll	ISP	2.052	-1.237	Pena-Herazo et al. (2021)

Table 6 *continued*

Table 6 *(continued)*

N (1)	4FGL name (2)	Class (3)	SED class (4)	Γ_{PH} (5)	logF_X (6)	references (7)
48	4FGL J0509.4+0542	bll	ISP	2.079	-0.328	Padovani et al. (2019)
49	4FGL J0430.3−2507	bll	ISP	2.176	-1.252	Shaw et al. 2012

Note—The number of the records are presented in Column 1. Column 2 lists the source name of 4FGL. The optical classes and the SED class reported in 4FGL are presented in Column 3 and Column 4, respectively, where "bll" indicates BL Lac and "fsrq" indicates FSRQ. The γ-ray photon spectral index (Γ_{PH}) and the X-band VLBI radio flux (log F_X) are shown in Columns 5 and 6; respectively. The references are listed in Columns 7. The simple horizontal line is used to distinguish the LSP BL Lacs, LSP FSRQs, and HSP (ISP) BL Lacs type TCLBs.

6. DISCUSSION AND CONCLUSION

Based on the 4LAC, 4FGL and RCF catalog, we constructed a sample containing 1680 Fermi sources with known EW-based (optical) classifications (FSRQs and BL Lacs) and SED-based classifications (LSP, ISP, and HSP). Which includes 651 FSRQs and 1029 BL Lacs, that are divided into 960 LSP, 334 ISP and 386 HSP sources. Where, 1352 blazars with 651 FSRQs and 701 ISP and HSP BL Lacs are viewed as the training and validation samples; All 328 LSP BL Lacs are viewed as a forecast sample. Approximately 4/5 of 1352 blazars are randomly (random seed = 123) assigned to the training sample, and the remaining ones (e.g., approximately 1/5) are considered as the validation sample. Here, the training sample include 1082 blazars with 528 FSRQs and 554 HSP (and LSP) BL Lacs, and the validation sample has 270 blazars with 123 FSRQs and 147 ISP, or HSP BL Lacs. Based on the D $>$ 0.300 in the two sample K-S test and Gini $>$ 2.000 in RF algorithm for all parameters with valid observations, there are 23 parameters selected in the work for the 1680 sources. Using the the RF algorithm with the default settings for the RF classification functions ($randomForest()$ in R code) to the selected sample (the training, validation and forecast samples), the 8388607 different combinations for the selected 23 parameters are calculated. There are 178 OPCs (the optimal parameters combinations) with a maximum accuracy (accuracy$\simeq$0.9889) are obtained, where, 1, 5, 14, 35, 52, 39, 28, 2, or 2 combinations of 5, 6, 7, 8, 9, 10, 11, 12, or 13 parameters (see Table 3), respectively. We select nine combinations, one combination in the combinations with 5, 6, 7, 8, 9, 10, 11, 12, or 13 parameters, respectively. Combined the classification results from the nine optimal combinations of parameters, 113 ABLLs and 157 possible CLBCs are predicted; however, 58 remain without a clear prediction; for 328 LSP BL Lacs reported in the high Galactic latitudes ($|b| > 10°$) 4LAC-DR2 catalog. Compared the predictions: between ABLLs and CLBCs, we found that the CLBC sources show a clear separation for ABLLs in the $logF_X$-Γ_{ph} plane, which can use a simple phenomenological critical line (see Equation 3 and Figure 2) to roughly separate these two subclasses, where, the CLBC sources are located in higher areas. Furthermore, the Γph of the CLBCs is slightly smaller than that of the FSRQs reported in 4LAC (green empty squares in right panel in Figure 3). Checked the TCLBs, there are 34 of 35 LSP TCLBs are located in the transition zone. Therefore, we propose a B-to-F transition zone named "$B \to F$" zone where the transition from BL Lac to FSRQ will occur for LSP BL Lac.

A portion of BL Lacs, which are essentially FSRQs, are misclassified as BL Lacs, vice versa. This peculiar rare transition phenomenon between BL Lacs and FSRQs (EW become larger or smaller) has been explored / addressed by many/some authors. There are some possible scenarios addressed the peculiar rare transitional phenomenon. Which is common addressed by some possible scenarios in the previous literature. For instance, the broad lines (EW) of some transition sources may be swamped by the strong (beamed) jet continuum variability (e.g., Vermeulen et al. 1995; Giommi et al. 2012; Ruan et al. 2014; Pasham & Wevers 2019), or jet bulk Lorentz factor variability (e.g., Bianchin et al. 2009a); Or some transition sources with weak radiative cooling, the broad lines are overwhelmed by the non-thermal continuum (e.g., Ghisellini et al. 2012). In addition, some strong broad lines of the FSRQ type source are missed due to with a high redshift (e.g., $z > 0.7$, D'Elia et al. 2015), the one of the strongest $H\alpha$ line falls outside the optical window, caused the misclassification. Also, several observational effects (e.g., signal-to- noise ratio, and spectral resolution, etc.) may also affected the optical classification (see Peña-Herazo et al. 2021a for the related discussions). In-depth research is of great significance to deepen the understanding of the origin of CLB sources, the accretion state transition of supermassive black holes; jet particle acceleration process; and black hole-galaxy co-evolution, etc (e.g., Ruan et al. 2014; Mishra 2021).

In section 5, the prediction results between our (C_9) predictions of this work using RF algorithm and the Fan's predictions (Fan & Wu 2019), CKZ's predictions (Cheng et al. 2022) or Paliya's Predictions (Paliya et al. 2021) are compared, respectively. Among the common objects through cross-matching, the prediction results of most of the sources are consistent (see Table 5). It suggests that our predictions are robust and effective. However, we should note that among the 1680 selected sample sources, there are 167 source X-band flux data missing in the training and validation sample and 30 source X-band flux data missing in the forecast sample. In the RF algorithm, the missing data is filled with the median using the na.roughfix() function of the RF algorithm. Based on a set of combined parameters, we test that the predictions of missing data with mean filling are basically consistent with that of with the median filling; We also tested, delete the source of missing data, the prediction results are basically the same. However, the prediction accuracy decreased slightly (accuracy $\simeq$0.9728), which basically had no effect on our main conclusions. Also, there are a total of 178 optimal parameters combinations (OPC) with a maximum accuracy and we select only 9 of these OPCs to combine and construct our prediction results (C_9 predictions, see Table 2 and 4). We also tried crossing more parameter combinations, the Predictions CLBCs and ABLLs had slightly fewer sources, and UNK sources had slightly more sources. From various combinations, we select only a part of them, which have a little effect on the final prediction result. In addition, some sources without SED classes were removed, possibly with selection effects. In the random forest calculation, the randomForest() function using the default setting, and the random factor is set as: seed=123, also slightly affect the forecast results (see Kang et al. 2019a for some related discussion), also need to note.

Moreover, we should note that we only address the transition from LSP BL Lacs to FSRQs in the work and only suggest a "$B \to F$" zone. Using the B-to-F transition zone, the LSP CLBCs can be well identified from LSP BL Lacs. Almost all the LSP BL Lac type TCLBs are located in the B-to-F transition region, only one source (4FGL J1503.5+4759 with Γ_{ph} = 2.221 and $logF_X$ = -1.319) are not in. But, the source is very close to the critical line. We also note that all the LSP FSRQ type TCLBs are also located in the B-to-F transition region (see Figure 3 in Section 5). One FSRQ type TCLBs, 4FGL J0134.5+2637, is not located in the "$B \to F$" zone, but, it is a HSP FSRQ type source. Which imply that these LSP FSRQ type TCLBs may be some LSP BL Lacs that have transitioned, may be BL Lacs before the transition (e.g., see Foschini et al. 2021, some FSRQs, featureless or weaker lines in previous literature). This also further indicates that the B-to-F transition zone can effectively screen out those potential CLBCs from LSP BL Lacs, which verifies the validity/ effectiveness of the B-to-F transition zone. In addition, vice versa, a transition from FSRQs to BL Lacs (F-to-B transition) is also possible. The possible candidates for the F-to-B transition that cannot be addressed only based on this work. Which needs to be further addressed in the future. When the F-to-B transition candidate sources are also screened, the F-to-B transition region can be effectively demarcated. Also, the complete CLBs (B$\rightleftarrows$F) transition region (B-to-F transition, Vice versa) may be proposed. And the role of CLB in the blazar sequence, its evolution (e.g., blazar redshift evolution), origin and other issues can be further discussed/ studied (Ruan et al. 2014). Also, the '$B \to F$' zone is obtained only based on the two parameters of the $logF_X$ and Γ_{ph}. For other parameters (or multi-dimensional parameter space) whether there are similar regions, or better discrimination, further research is needed.

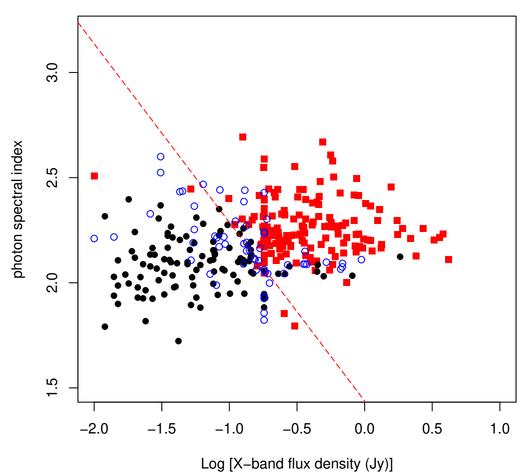

Figure 4. Scatterplots for the photon spectral index (Γ_{PH}) and the X-band flux (log F_X), where the black filled circles, red solid squares, and blue empty circles indicate ABLLs, CLBCs and UNKs respectively.

We also should note that there are 58 UNK sources without a clear prediction (see Table 4). They are scattered on both sides of the critical line (see Figure 4). The boundary between CLBCs and ABLLs is simply distinguished employed a straight line, which is a bit too simple and seems a bit unreasonable. Complex separation boundaries (or multi-dimensional parameter space) may be more realistic and effective, which needed to be further addressed. The LSP TCLB source: 4FGL J1503.5+4759 is not located in the B-to-F transition zone, but, the source is very close to the critical line. Combined with the distribution characteristics of 58 UNK sources, it seems imply that there are more complex separation boundaries. Whether the assumption is reasonable and whether it exists requires further research.

Although there are still many deficiencies in our work, our work may be still effective in diagnosing the possible of CLBC sources from LSP BL Lacs. For extremely rare CLB sources, our work will greatly enrich the sample of CLB sources, which would influence the study of different properties between BL Lacs and FSRQs, especially regarding the role of CLB sources in the evolution of blazar sequences, or their redshift evolution, etc., and provide abundant samples. It would also provide potentially valid target sources for the discovery of additional CLB sources and for subsequent confirmation of CLB sources, especially future large spectroscopic or photometric surveys (e.g., **check some surveys**). This issue will continue to be addressed in future work.

7. ACKNOWLEDGMENT

We thanks the anonymous editor and referee for very constructive and helpful comments and suggestions, which greatly helped us to improve our paper. We also thanks all the people that have made this work what it is today. This includes but not limited to K. R. Zhu, and R. X. Zhou, S. S. Ren. Also special thanks to Xu-Liang Fan and Yi-Ping Cheng for providing their predictions. And we would like to express our gratitude to EditSprings (https://www.editsprings.com/) for the expert linguistic services provided. This work is partially supported by the National Natural Science Foundation of China (Grant Nos. 12163002, 11873043 and, U1931203, U2031201), and the big data astronomy and physics science and technology innovation team of Liupanshui Normal University（LPSSYKJTD201901）

Facilities: Fermi (LAT), VLBI (RFC)

Software: R (R Core Team 2022), randomForest (Liaw & Wiener 2002), e1071 (Meyer et al. 2021), snowfall (Knaus 2015)

APPENDIX

A. AN ONLINE CHANGING-LOOK (TRANSITION) BLAZARS CATALOG

The changing-look (transition) blazars (TCLBs) are the source that there are optical spectra at different epochs showing significant changes. These sources present a clear transition between the standard FSRQs and BL Lac types. Here, a new online interactive catalog for the TCLBs (CLBsCat[11]) is presented. Currently, the TCLBs are extremely rare astronomical objects. As CLB sources (transition sources) continue to grow, CLBsCat may provide the global astrophysics community with easy, timely and comprehensive information on this rapidly developing field.

At present, the CLBsCat has not been fully publicly released, and is only available online at http://orcid.org/0000-0002-9071-5469 for a web link: https://github.com/ksj7924/CLBCat for the convenience of everyone to view, modify and improve until the application is permanently fixed in a network space. Community groups or individuals are welcome to contribute or provide a suitable network for the joint development.

A.1. *The TCLBs in Foschini et al. (2021)*

Foschini et al. (2021) compiled a gamma-ray jetted AGN sample based on the 4FGL catalog. They reported 11 changing-look AGNs, based on a featureless spectrum reported in the previous literature (see Foschini et al. 2021 for more details and references therein). Where, 9 of them are blazars labeled as FSRQ in 4FGL catalog, one of them is

[11] https://github.com/ksj7924/CLBCat/

non-blazar active galaxy labeled as "agn" in 4FGL catalog, and one of them is compact steep spectrum radio source labeled as "css" in 4FGL catalog.

The 11 sources are listed in Table A.1.

Table A.1. The TCLBs in Foschini et al. (2021)

4FGL name (1)	R.A. (2)	Decl. (3)	ASSOC name (4)	SED class (5)	4FGL Class (6)	From class (7)	To class (8)
4FGL J0134.5+2637	23.6272	26.6294	RX J0134.4+2638	HSP	fsrq	featureless	fsrq
4FGL J0217.8+0144	34.4621	1.7346	PKS 0215+015	LSP	fsrq	featureless	fsrq
4FGL J0449.1+1121	72.2823	11.3569	PKS 0446+11	LSP	fsrq	featureless	fsrq
4FGL J0509.4+1012	77.3510	10.2008	PKS 0506+101	LSP	fsrq	featureless	fsrq
4FGL J0510.0+1800	77.5181	18.0135	PKS 0507+17	LSP	fsrq	featureless	fsrq
4FGL J0522.9−3628	80.7370	-36.4686	PKS 0521−36	LSP	agn	featureless	agn
4FGL J0719.3+3307	109.8400	33.1232	B2 0716+33	LSP	fsrq	featureless	fsrq
4FGL J0833.9+4223	128.4759	42.3989	OJ 451	LSP	fsrq	featureless	fsrq
4FGL J0910.0+4257	137.5058	42.9623	3C 216	...	css	featureless	css
4FGL J1037.4−2933	159.3564	-29.5568	PKS 1034−293	LSP	fsrq	featureless	fsrq
4FGL J1124.0+2336	171.0045	23.6159	OM 235	LSP	fsrq	featureless	fsrq

Note—The 4FGL name are presented in Column 1. Columns 2 and 3 are the J2000 coordinates. The counterpart names are listed in Column 4. Column 5 and 6 lists the spectral energy distribution (SED) class and the optical class reported in 4FGL catalog, respectively. The optical class before and after the transition in Foschini et al. (2021) are presented in Columns 7 and 8, respectively.

A.2. *The TCLBs in Peña-Herazo et al. (2021a)*

In Peña-Herazo et al. (2021a), they reported 26 Changing-Look (transitional) blazars (TCLBs) that changed their classification. Six of them are confirmed that are the blazar-like nature of BL Lac candidates. All remaining sources followed with previous classifications.

Which are listed in Table A.2.

Table A.2. The TCLBs in Peña-Herazo et al. (2021a)

4FGL name (1)	R.A. (2)	Decl. (3)	SED class (4)	4FGL Class (5)	ASSOC name (6)	From class (7)	To class (8)
4FGL J1410.3+1438	212.5908	14.6434	...	bll	4FGL J1410.3+1438	bll	bzq
4FGL J1503.5+4759	225.8955	47.9959	LSP	bll	4FGL J1503.5+4759	bll	bzq
...	...	...	...	...	SDSS J134240.02+094752.4	bzq	bzb
...	...	...	...	...	5BZG J0006+1051	bzg	bzb
4FGL J0022.0+0006	5.5154	0.1134	HSP	bll	5BZG J0022+0006	bzg	bzb
4FGL J0303.3+0555	45.8465	5.9249	HSP	bll	5BZG J0303+0554	bzg	bzb
...	...	...	...	...	5BZG J0751+1730	bzg	bzq

Table A.2 *continued*

Table A.2 *(continued)*

4FGL name (1)	R.A. (2)	Decl. (3)	SED class (4)	4FGL Class (5)	ASSOC name (6)	From class (7)	To class (8)
...	...	...	...	...	5BZG J0756+3834	bzg	bzq
4FGL J0916.7+5238	139.1906	52.6454	HSP	bll	5BZG J0916+5238	bzg	bzb
4FGL J1001.1+2911	150.2938	29.1880	LSP	bll	5BZB J1001+2911	bzb	bzq
4FGL J1043.2+2408	160.8053	24.1460	LSP	fsrq	5BZQ J1043+2408	bzq	bzb
...	...	...	...	...	5BZQ J1054+3855	bzq	bzb
4FGL J1056.0+0253	164.0027	2.8935	...	bll	5BZG J1056+0252	bzg	bzb
...	...	...	...	...	5BZG J1103+0022	bzg	bzb
4FGL J1106.0+2813	166.5020	28.2254	LSP	fsrq	5BZQ J1106+2812	bzq	bzb
...	...	...	...	...	5BZQ J1243+4043	bzq	bzb
4FGL J1321.1+2216	200.2958	22.2808	LSP	fsrq	5BZQ J1321+2216	bzq	bzb
4FGL J1326.1+1232	201.5493	12.5348	HSP	bll	5BZG J1326+1229	bzg	bzb
...	...	...	...	...	5BZQ J1343+2844	bzq	bzb
4FGL J1402.6+1600	210.6584	16.0016	ISP	bll	5BZB J1402+1559	bzb	bzq
4FGL J1449.5+2746	222.3956	27.7686	ISP	rdg	5BZG J1449+2746	bzg	bzb
...	...	...	...	...	5BZG J1504−0248	bzg	bzq
4FGL J1512.2+0202	228.0702	2.0403	LSP	fsrq	5BZG J1512+0203	bzg	bzq
4FGL J1730.8+3715	262.7026	37.2641	ISP	bll	5BZG J1730+3714	bzg	bzb
...	...	...	...	...	5BZG J1733+4519	bzg	bzb
...	...	...	...	...	5BZG J2346+4024	bzg	bzq

Note—The 4FGL name are presented in Column 1. Columns 2 and 3 are the J2000 coordinates. Column 4 is the spectral energy distribution (SED) class and Column 5 lists the optical class reported in 4FGL catalog, respectively. The counterpart names are listed in Column 6. The optical class before and after the transition in Peña-Herazo et al. (2021a) are presented in Columns 7 and 8, respectively. Where, BL lacs labeled as BZB and FSRQs labeled as BZQ (or BZG) in the Roma-BZCAT.

A.3. *The TCLBs in Ruan et al. (2014)*

Based on the EW of their optical broad emission lines, blazars are common classically divided into the BL Lacs and FSRQs subclasses. The EW-based classification criteria are not physically motivated, and some blazars have previously "transitioned" from one subclass to the other. In Ruan et al. (2014), they present the first systematic search for these transition blazars in a sample of 602 unique pairs of repeat spectra of 354 blazars in the Sloan Digital Sky Survey, finding six clear transition blazars.

Which are listed in Table A.3.

Table A.3. The TCLBs in Ruan et al. (2014)

4FGL name (1)	R.A. (2)	Decl. (3)	SED class (4)	4FGL Class (5)	ASSOC name (6)	From class (7)	To class (8)
4FGL J0833.9+4223	128.4759	42.3989	LSP	fsrq	SDSS J083353.88+422401.8	P−BLL	FSRQ−like
4FGL J1016.0+0512	154.0093	5.2089	LSP	fsrq	SDSS J101603.13+051302.3	P−BLL	FSRQ−like

Table A.3 *continued*

Table A.3 *(continued)*

4FGL name (1)	R.A. (2)	Decl. (3)	SED class (4)	4FGL Class (5)	ASSOC name (6)	From class (7)	To class (8)
4FGL J1308.5+3547	197.1286	35.7918	LSP	fsrq	SDSS J130823.70+354637.0	P−BLL	FSRQ−like
4FGL J2206.8−0032	331.7087	-0.5461	LSP	bll	SDSS J220643.28−003102.5	P−BLL	FSRQ−like
4FGL J1250.6+0217	192.6513	2.2876	LSP	bll	SDSS J125032.57+021632.1	P−BLL	FSRQ−like
...	...	...	...	...	SDSS J143758.67+300207.1	P−BLL	FSRQ−like

Note—The 4FGL name are presented in Column 1. Columns 2 and 3 are the J2000 coordinates. Column 4 lists the spectral energy distribution (SED) class and column 5 lists the optical class reported in 4FGL catalog, respectively. The counterpart names are listed in Column 6. The optical class before and after the transition in Ruan et al. (2014) are presented in Columns 7 and 8.

A.4. *The TCLBs in Shaw et al. (2012)*

In Shaw et al. 2012, they found that some blazars were classified as BL Lacs in initial epoch observations. However, in some spectral observation periods, where the continuum is low, and they all show broad lines as FSRQ-type sources. In addition, some BL Lacs with very high S/N observations that the broad lines were detected at high significance at EW levels < 5Å. These were thus "BL Lac objects" can be analyzed along with the FSRQ. They suggested that these sources present a clear transitional between the standard FSRQs and BL Lac types

Which are listed in Table A.4

Table A.4. The 11 TCLB sources in Shaw et al. (2012)

4FGL name (1)	R.A. (2)	Decl. (3)	SED class (4)	4FGL Class (5)	ASSOC name (6)	From class (7)	To class (8)
4FGL J0058.4+3315	14.6101	33.2505	LSP	fsrq	1FGL J0058.0+3314	BL Lac	nominal_FSRQ
4FGL J0923.5+4125	140.8949	41.4283	LSP	fsrq	1FGL J0923.2+4121	BL Lac	nominal_FSRQ
4FGL J1001.1+2911	150.2938	29.1880	LSP	bll	1FGL J1000.9+2915	BL Lac	nominal_FSRQ
4FGL J1607.0+1550	241.7745	15.8447	LSP	bll	1FGL J1607.1+1552	BL Lac	nominal_FSRQ
4FGL J2032.0+1219	308.0040	12.3279	LSP	bll	1FGL J2031.5+1219	BL Lac	nominal_FSRQ
4FGL J2244.2+4057	341.0614	40.9597	LSP	fsrq	1FGL J2243.4+4104	BL Lac	nominal_FSRQ
4FGL J0430.3−2507	67.5751	-25.1283	ISP	bll	1FGL J0430.4−2509	BL Lac	broad_lines_BLL
4FGL J0516.7−6207	79.1798	-62.1248	LSP	bll	1FGL J0516.7−6207	BL Lac	broad_lines_BLL
4FGL J1058.4+0133	164.6240	1.5641	LSP	bll	1FGL J1058.4+0134	BL Lac	broad_lines_BLL
4FGL J2236.3+2828	339.0962	28.4832	LSP	fsrq	1FGL J2236.2+2828	BL Lac	broad_lines_BLL
4FGL J2315.6−5018	348.9140	-50.3127	LSP	bll	1FGL J2315.9−5014	BL Lac	broad_lines_BLL

Note—The 4FGL name are presented in Column 1. Columns 2 and 3 are the J2000 coordinates. Column 4 is the spectral energy distribution (SED) class and Column 5 lists the optical class reported in 4FGL catalog, respectively. The 1FGL counterpart names are listed in Column 6. The optical class before and after the transition in Shaw et al. (2012) are presented in Columns 7 and 8, respectively.

A.5. *The TCLBs in Ghisellini et al. (2011)*

In Ghisellini et al. (2011), they suggested that some sources classified as BL Lacs with an SED appearing as intermediate between BL Lacs and FSRQs also have relatively weak broad emission lines and small EW, and can be considered as transition sources

Which are listed in Table A.5.

Table A.5. The TCLB sources in Ghisellini et al. (2011)

4FGL name (1)	R.A. (2)	Decl. (3)	ASSOC name (4)	SED class (5)	4FGL Class (6)	From class (7)	To class (8)
4FGL J0058.4+3315	14.6101	33.2505	MG3 J005830+3311	LSP	fsrq	BL Lacs	FS
4FGL J0210.7−5101	32.6946	-51.0218	PKS 0208−512	LSP	fsrq	BL Lacs	FS
4FGL J0538.8−4405	84.7089	-44.0862	PKS 0537−441	LSP	bll	BL Lacs	FS
4FGL J0811.4+0146	122.8610	1.7756	OJ 014.	LSP	bll	BL Lacs	FS
4FGL J0238.6+1637	39.6680	16.6179	PKS 0235+164	LSP	bll	BL Lacs	FS
4FGL J0428.6−3756	67.1730	-37.9403	PKS 0426−380	LSP	bll	BL Lacs	FS

NOTE—The 4FGL name are presented in Column 1. Columns 2 and 3 are the J2000 coordinates. The counterpart names are listed in Column 4. Column 5 is the spectral energy distribution (SED) class and column 6 lists the optical class reported in 4FGL catalog, respectively. The optical class before and after the transition in Ghisellini et al. (2011) are presented in Columns 7 and 8.

A.6. *The TCLBs in other literatures*

Some other individual TCLBs reported in some literatures (Vermeulen et al. 1995; Mishra et al. 2021; Álvarez Crespo et al. 2016; Pasham & Wevers 2019; Cutini et al. 2014; Padovani et al. 2019; Bianchin et al. 2009b, etc. to be added and updated.) that listed in Table A.6.

Table A.6. The TCLB sources in other literatures

4FGL name (1)	R.A. (2)	Decl. (3)	SED class (4)	4FGL Class (5)	ASSOC name (6)	From class (7)	To class (8)	ref. (9)
4FGL J2202.7+4216	330.6946	42.2821	LSP	bll	BL Lac (prototype)	BL Lac	FSRQ	[a]
4FGL J1422.3+3223	215.5772	32.3911	LSP	fsrq	B2 1420+32	FSRQ	BL Lac	[b]
...	...	...	...	...	5BZB J0724+2621	BL Lac	FSRQ.	[c]
...	...	...	...	...	J211354.71+112125.3.	FSRQ	no BELs.	[d]
4FGL J1153.4+4931	178.3505	49.5169	LSP	fsrq	4C+29.22 (S4 1150+49)	FSRQ	BL Lacs	[e]
4FGL J0509.4+0542	77.3593	5.7014	ISP	bll	TXS 0506+056	bll	FSRQ	[f]
4FGL J2151.8−3027	327.9655	-30.4600	LSP	fsrq	PKS 2149−306			[g]

Table A.6 *continued*

Table A.6 *(continued)*

4FGL name	R.A.	Decl.	SED class	4FGL Class	ASSOC name	From class	To class	ref.
(1)	(2)	(3)	(4)	(5)	(6)	(7)	(8)	(9)

Note—The 4FGL name are presented in Column 1. Columns 2 and 3 are the J2000 coordinates. Column 4 is the spectral energy distribution (SED) class and column 5 lists the optical class reported in 4FGL catalog, respectively. The counterpart names are listed in Column 6. The optical class before and after the transition in Ghisellini et al. (2011) are presented in Columns 7 and 8, respectively. Where,
[a] Vermeulen et al. (1995); based on optical line.
[b] Mishra et al. (2021); based on optical line.
[c] Álvarez Crespo et al. (2016); based on optical line.
[d] Pasham & Wevers (2019); based on optical line.
[e] Cutini et al. (2014); based on SED.
[f] Padovani et al. (2019); based on Eddington ratio.
[g] Bianchin et al. (2009b). based on SED.

A portion of data and/or tables is shown here for guidance regarding its form and content (All the data tables is available in its entirety on https://github.com/ksj7924/CLBCat). Other data and/or tables, including but not limited to, the confirmed CLBs, the predicted CLBs; and these transitional blazars, or the possible transitional blazars between the standard FSRQs and BL Lac types (EW-based classification); even also including the red or blue (quasars) blazars; and broad line BL Lac types sources, also can be found on the online catalog: CLBsCat https://github.com/ksj7924/CLBCat.

REFERENCES

Abdo, A. A., Ackermann, M., Agudo, I., et al. 2010a, ApJ, 716, 30, doi: 10.1088/0004-637X/716/1/30

Abdo, A. A., Ackermann, M., Ajello, M., et al. 2010b, ApJS, 188, 405, doi: 10.1088/0067-0049/188/2/405

—. 2010c, ApJ, 715, 429, doi: 10.1088/0004-637X/715/1/429

Abdollahi, S., Acero, F., Ackermann, M., et al. 2020, ApJS, 247, 33, doi: 10.3847/1538-4365/ab6bcb

Abdollahi, S., Acero, F., Baldini, L., et al. 2022, ApJS, 260, 53, doi: 10.3847/1538-4365/ac6751

Acero, F., Ackermann, M., Ajello, M., et al. 2015, ApJS, 218, 23, doi: 10.1088/0067-0049/218/2/23

Ackermann, M., Ajello, M., Allafort, A., et al. 2011, ApJ, 743, 171, doi: 10.1088/0004-637X/743/2/171

—. 2012, ApJ, 753, 83, doi: 10.1088/0004-637X/753/1/83

Ackermann, M., Ajello, M., Atwood, W. B., et al. 2015, ApJ, 810, 14, doi: 10.1088/0004-637X/810/1/14

Acuner, Z., & Ryde, F. 2018, MNRAS, 475, 1708, doi: 10.1093/mnras/stx3106

Ajello, M., Angioni, R., Axelsson, M., et al. 2020, ApJ, 892, 105, doi: 10.3847/1538-4357/ab791e

Álvarez Crespo, N., Masetti, N., Ricci, F., et al. 2016, AJ, 151, 32, doi: 10.3847/0004-6256/151/2/32

Ballet, J., Burnett, T. H., Digel, S. W., & Lott, B. 2020, arXiv e-prints, arXiv:2005.11208. https://arxiv.org/abs/2005.11208

Baron, D. 2019, arXiv e-prints, arXiv:1904.07248. https://arxiv.org/abs/1904.07248

Beasley, A. J., Gordon, D., Peck, A. B., et al. 2002, ApJS, 141, 13, doi: 10.1086/339806

Bhattacharya, D., Sreekumar, P., Mukhopadhyay, B., & Tomar, I. 2016, Research in Astronomy and Astrophysics, 16, 54, doi: 10.1088/1674-4527/16/4/054

Bianchin, V., Foschini, L., Ghisellini, G., et al. 2009a, A&A, 496, 423, doi: 10.1051/0004-6361/200811128

—. 2009b, A&A, 496, 423, doi: 10.1051/0004-6361/200811128

Böttcher, M. 2019, Galaxies, 7, 20, doi: 10.3390/galaxies7010020

Boula, S., Kazanas, D., & Mastichiadis, A. 2019, MNRAS, 482, L80, doi: 10.1093/mnrasl/sly189

Breiman, L. 2001, Machine Learning, 45, 5, doi: 10.1023/A:1010933404324

Breiman, L., Last, M., & Rice, J. 2003, in Statistical Challenges in Astronomy, ed. E. D. Feigelson & G. J. Babu, 243–254

Cao, X. 2002, ApJL, 570, L13, doi: 10.1086/340855

—. 2003, ApJ, 599, 147, doi: 10.1086/379240

Capetti, A., Raiteri, C. M., & Buttiglione, S. 2010, A&A, 516, A59, doi: 10.1051/0004-6361/201014232

Chen, L. 2018, ApJS, 235, 39, doi: 10.3847/1538-4365/aab8fb

Chen, Y.-Y., Zhang, X., Xiong, D., & Yu, X. 2015, AJ, 150, 8, doi: 10.1088/0004-6256/150/1/8

Cheng, Y. P., Kang, S. J., & Zheng, Y. G. 2022, MNRAS, 515, 2215, doi: 10.1093/mnras/stac1885

Cheng, Y. P., Kang, S. J., & Zheng, Y. G. 2022, Monthly Notices of the Royal Astronomical Society, 515, 2215, doi: 10.1093/mnras/stac1885

Corbett, E. A., Robinson, A., Axon, D. J., et al. 1996, MNRAS, 281, 737, doi: 10.1093/mnras/281.3.737

Cutini, S., Ciprini, S., Orienti, M., et al. 2014, MNRAS, 445, 4316, doi: 10.1093/mnras/stu2011

Dai, H., Xie, G. Z., Zhou, S. B., et al. 2007, AJ, 133, 2187, doi: 10.1086/511769

D'Elia, V., Padovani, P., Giommi, P., & Turriziani, S. 2015, MNRAS, 449, 3517, doi: 10.1093/mnras/stv573

Doert, M., & Errando, M. 2014, ApJ, 782, 41, doi: 10.1088/0004-637X/782/1/41

Fan, J. H., Yang, J. H., Liu, Y., et al. 2016, ApJS, 226, 20, doi: 10.3847/0067-0049/226/2/20

Fan, X.-L., & Wu, Q. 2019, ApJ, 879, 107, doi: 10.3847/1538-4357/ab25f1

Feigelson, E. D., & Babu, G. J. 2012, Modern Statistical Methods for Astronomy

Fernández-Delgado, M., Cernadas, E., Barro, S., & Amorim, D. 2014, Journal of Machine Learning Research, 15, 3133. http://jmlr.org/papers/v15/delgado14a.html

Fomalont, E. B., Petrov, L., MacMillan, D. S., Gordon, D., & Ma, C. 2003, AJ, 126, 2562, doi: 10.1086/378712

Foschini, L., Lister, M. L., Antón, S., et al. 2021, Universe, 7, 372, doi: 10.3390/universe7100372

Gardner, E., & Done, C. 2018, MNRAS, 473, 2639, doi: 10.1093/mnras/stx2516

Ghisellini, G. 2016, Galaxies, 4, 36, doi: 10.3390/galaxies4040036

Ghisellini, G., Celotti, A., Fossati, G., Maraschi, L., & Comastri, A. 1998, MNRAS, 301, 451, doi: 10.1046/j.1365-8711.1998.02032.x

Ghisellini, G., Maraschi, L., & Tavecchio, F. 2009, MNRAS, 396, L105, doi: 10.1111/j.1745-3933.2009.00673.x

Ghisellini, G., Righi, C., Costamante, L., & Tavecchio, F. 2017, MNRAS, 469, 255, doi: 10.1093/mnras/stx806

Ghisellini, G., Tavecchio, F., Foschini, L., & Ghirlanda, G. 2011, MNRAS, 414, 2674, doi: 10.1111/j.1365-2966.2011.18578.x

Ghisellini, G., Tavecchio, F., Foschini, L., et al. 2012, MNRAS, 425, 1371, doi: 10.1111/j.1365-2966.2012.21554.x

Giommi, P., Padovani, P., & Polenta, G. 2013, MNRAS, 431, 1914, doi: 10.1093/mnras/stt305

Giommi, P., Padovani, P., Polenta, G., et al. 2012, MNRAS, 420, 2899, doi: 10.1111/j.1365-2966.2011.20044.x

Kabacoff, R. 2015, R in Action, Second Edition (Manning Publications Co.). http://www.allitebooks.com/r-in-action-second-edition/

Kang, S.-J., Fan, J.-H., Mao, W., et al. 2019a, ApJ, 872, 189, doi: 10.3847/1538-4357/ab0383

Kang, S.-J., Li, E., Ou, W., et al. 2019b, ApJ, 887, 134, doi: 10.3847/1538-4357/ab558b

Kang, S.-J., Zhu, K., Feng, J., et al. 2020, ApJ, 891, 87, doi: 10.3847/1538-4357/ab722d

Keenan, M., Meyer, E. T., Georganopoulos, M., Reddy, K., & French, O. J. 2021, MNRAS, 505, 4726, doi: 10.1093/mnras/stab1182

Knaus, J. 2015, snowfall: Easier cluster computing (based on snow). https://CRAN.R-project.org/package=snowfall

Landt, H., Padovani, P., Perlman, E. S., & Giommi, P. 2004, MNRAS, 351, 83, doi: 10.1111/j.1365-2966.2004.07750.x

Liaw, A., & Wiener, M. 2002, R News, 2, 18. https://CRAN.R-project.org/doc/Rnews/

Linford, J. D., Taylor, G. B., & Schinzel, F. K. 2012, ApJ, 757, 25, doi: 10.1088/0004-637X/757/1/25

Lott, B., Gasparrini, D., & Ciprini, S. 2020, arXiv e-prints, arXiv:2010.08406. https://arxiv.org/abs/2010.08406

Meyer, D., Dimitriadou, E., Hornik, K., Weingessel, A., & Leisch, F. 2021, e1071: Misc Functions of the Department of Statistics, Probability Theory Group (Formerly: E1071), TU Wien. https://CRAN.R-project.org/package=e1071

Mishra, H. 2021, in American Astronomical Society Meeting Abstracts, Vol. 53, American Astronomical Society Meeting Abstracts, 408.07

Mishra, H. D., Dai, X., Chen, P., et al. 2021, ApJ, 913, 146, doi: 10.3847/1538-4357/abf63d

Mondal, T., & Mukhopadhyay, B. 2019, MNRAS, 486, 3465, doi: 10.1093/mnras/stz1062

Nolan, P. L., Abdo, A. A., Ackermann, M., et al. 2012, ApJS, 199, 31, doi: 10.1088/0067-0049/199/2/31

Padovani, P., & Giommi, P. 2015, MNRAS, 446, L41, doi: 10.1093/mnrasl/slu164

Padovani, P., Oikonomou, F., Petropoulou, M., Giommi, P., & Resconi, E. 2019, MNRAS, 484, L104, doi: 10.1093/mnrasl/slz011

Paliya, V. S., Domínguez, A., Ajello, M., Olmo-García, A., & Hartmann, D. 2021, ApJS, 253, 46, doi: 10.3847/1538-4365/abe135

Pasham, D. R., & Wevers, T. 2019, Research Notes of the American Astronomical Society, 3, 92, doi: 10.3847/2515-5172/ab304a

Peña-Herazo, H. A., Massaro, F., Gu, M., et al. 2021a, AJ, 161, 196, doi: 10.3847/1538-3881/abe41d

—. 2021b, AJ, 162, 76, doi: 10.3847/1538-3881/ac09e2

Pei, Z., Fan, J., Yang, J., Huang, D., & Li, Z. 2022, ApJ, 925, 97, doi: 10.3847/1538-4357/ac3aeb

Petrov, L. 2021, AJ, 161, 14, doi: 10.3847/1538-3881/abc4e1

Prandini, E., & Ghisellini, G. 2022, Galaxies, 10, 35, doi: 10.3390/galaxies10010035

R Core Team. 2022, R: A Language and Environment for Statistical Computing, R Foundation for Statistical Computing, Vienna, Austria. https://www.R-project.org/

Ruan, J. J., Anderson, S. F., Plotkin, R. M., et al. 2014, ApJ, 797, 19, doi: 10.1088/0004-637X/797/1/19

Saz Parkinson, P. M., Xu, H., Yu, P. L. H., et al. 2016, ApJ, 820, 8, doi: 10.3847/0004-637X/820/1/8

Sbarrato, T., Ghisellini, G., Maraschi, L., & Colpi, M. 2012, MNRAS, 421, 1764, doi: 10.1111/j.1365-2966.2012.20442.x

Sbarrato, T., Padovani, P., & Ghisellini, G. 2014, MNRAS, 445, 81, doi: 10.1093/mnras/stu1759

Shaw, M. S., Romani, R. W., Cotter, G., et al. 2012, ApJ, 748, 49, doi: 10.1088/0004-637X/748/1/49

Stern, B. E., & Poutanen, J. 2014, ApJ, 794, 8, doi: 10.1088/0004-637X/794/1/8

Stickel, M., Padovani, P., Urry, C. M., Fried, J. W., & Kuehr, H. 1991, ApJ, 374, 431, doi: 10.1086/170133

Stocke, J. T., Morris, S. L., Gioia, I. M., et al. 1991, ApJS, 76, 813, doi: 10.1086/191582

Taylor, M. B. 2005, in Astronomical Society of the Pacific Conference Series, Vol. 347, Astronomical Data Analysis Software and Systems XIV, ed. P. Shopbell, M. Britton, & R. Ebert, 29

Urry, C. M., & Padovani, P. 1995, PASP, 107, 803, doi: 10.1086/133630

Vermeulen, R. C., Ogle, P. M., Tran, H. D., et al. 1995, ApJL, 452, L5, doi: 10.1086/309716

Wang, J.-M., Staubert, R., & Ho, L. C. 2002, ApJ, 579, 554, doi: 10.1086/342875

Xu, Y.-D., Cao, X., & Wu, Q. 2009, ApJL, 694, L107, doi: 10.1088/0004-637X/694/2/L107

Yuan, F., & Narayan, R. 2014, ARA&A, 52, 529, doi: 10.1146/annurev-astro-082812-141003

Zhang, L., Liu, Y., & Fan, J. 2022, ApJ, 935, 4, doi: 10.3847/1538-4357/ac7bde

Zhu, K. R., Kang, S. J., Zhou, R. X., & Zheng, Y. G. 2021, ApJ, 916, 93, doi: 10.3847/1538-4357/ac088c